World Electric Vehicle Journal

MDPI

Article

Intricate DG and EV Planning Impact Assessment with Seasonal Variation in a Three-Phase Distribution System

Abhinav Kumar [1], Sanjay Kumar [1], Umesh Kumar Sinha [1] and Aashish Kumar Bohre [2,*]

[1] Electrical Engineering Department, National Institute of Technology, Jamshedpur 831014, India; iitkgp.ab@gmail.com (A.K.); sanjay.ee@nitjsr.ac.in (S.K.); uksinha.ee@nitjsr.ac.in (U.K.S.)
[2] Electrical Engineering Department, National Institute of Technology, Durgapur 713209, India
* Correspondence: aashishkumar.bohre@ee.nitdgp.ac.in

Abstract: Modern power systems present opportunities and challenges when integrating distributed generation and electric vehicle charging stations into unbalanced distribution networks. The performance and efficiency of both Distributed Generation (DG) and Electric Vehicle (EV) infrastructure are significantly affected by global temperature variation characteristics, which are taken into consideration in this study as it investigates the effects of these integrations. This scenario is further complicated by the unbalanced structure of distribution networks, which introduces inequalities that can enhance complexity and adverse effects. This paper analyzes the manner in which temperature changes influence the network operational voltage profile, power quality, energy losses, greenhouse harmful emissions, cost factor, and active and reactive power losses using analytical and heuristic techniques in the IEEE 69 bus network in both three-phase balance and modified unbalanced load conditions. In order to maximize adaptability and efficiency while minimizing the adverse impacts on the unbalanced distribution system, the findings demonstrate significant variables to take into account while locating the optimal location and size of DG and EV charging stations. To figure out the objective, three-phase distribution load flow is utilized by the particle swarm optimization technique. Greenhouse gas emissions dropped by 61.4%, 64.5%, and 60.98% in each of the three temperature case circumstances, while in the modified unbalanced condition, they dropped by 57.55%, 60.39%, and 62.79%. In balanced conditions, energy loss costs are reduced by 95.96%, 96.01%, and 96.05%, but in unbalanced conditions, they are reduced by 91.79%, 92.06%, and 92.46%. The outcomes provide valuable facts that electricity companies, decision-makers, along with other energy sector stakeholders may utilize to formulate strategies that adapt to the fluctuating patterns of electricity distribution during fluctuations in global temperature under balanced and unbalanced conditions of network.

Keywords: integrated renewable distributed generation; balanced and unbalanced distribution system; electrical vehicles charging corridors; active and reactive power loss; voltage profile; greenhouse gas emissions; particle swarm optimization

Citation: Kumar, A.; Kumar, S.; Sinha, U.K.; Bohre, A.K. Intricate DG and EV Planning Impact Assessment with Seasonal Variation in a Three-Phase Distribution System. *World Electr. Veh. J.* **2024**, *15*, 425. https://doi.org/10.3390/wevj15090425

Academic Editors: Wenming Yang and Anna Pinnarelli

Received: 15 July 2024
Revised: 7 September 2024
Accepted: 11 September 2024
Published: 19 September 2024

1. Introduction

Integrated EVs and DGs are new technology advancements that were developed to address environmental concerns. They reduce air pollution, which accounts for all greenhouse gas emissions. The number of EVs sold in the US and the UK is increasing at an exponential rate, with 2 million EVs sold in 2016, 40 million in 2020, and 70 million predicted to be sold by 2025 [1]. They emphasize interoperability and compliance with global standards, addressing critical considerations for the development of robust and interoperable EV charging infrastructure. Kathiravan et al. [2] proposed using the Ant Lion Optimizer algorithm to optimize the location of Electric Vehicle Charging Station (EVCS) while minimizing line losses. They deliver an innovative approach that considers the technical and financial aspects of EVCS adoption. The authors in [3] designed an effective energy management

system for EVCSs and the electricity distribution system. They prioritized the usage of renewable energy resources while maintaining dependable EV charging infrastructure. Ahmad et al. [4] reviewed the ideal location of EVCSs and their impact on distribution networks. Their research sheds light on the problems and opportunities that come with EVCS adoption, taking into account variables like grid dependability and environmental sustainability. In [5], a unique AI approach was developed for the efficient deployment of EV fast charging stations in distribution networks, combining AI approaches with solar-based distributed generation systems to improve the dependability and efficiency of EV charging infrastructure. In [6], the authors addressed the topic of increasing the hosting capacity of unbalanced distribution networks for Distributed Energy resources (DERs) via efficient load re-phasing. The authors emphasize the necessity of grid flexibility in handling the growing number of EVs and other Ders. In [7], a novel probabilistic methodology to plan for EVCs in distribution is presented, taking into account spatiotemporal uncertainty. Their technique addresses an important part of EV infrastructure development, offering useful insights into minimizing uncertainty related to EV charging demand and grid integration. Harish et al. [8] provide a comprehensive overview of power quality challenges originating from the integration of EV into distribution systems. They offer an informative study of difficulties such as harmonics, voltage fluctuations, and unbalance, as well as mitigating approaches to assure grid stability and reliability. Ahmad et al. [9] proposed an improved method for optimally placing solar-powered electric vehicle charging stations in distribution networks. Their study provides valuable insights into using renewable energy sources for sustainable EV infrastructure development and contributes to decarbonizing transportation. Eid et al. [10] focused on the successful operation of BES devices, electric car charging stations, and renewable-based energy sources that are linked to Distribution Network (DN). Their research sheds light on the synergistic integration of these components to improve grid resilience, promote renewable energy utilization, and support EV charging infrastructure. Islam et al. [11] proposed a coordinated EV charging strategy that takes into account correlated EV and grid loads, as well as photovoltaic output variability. Their study introduces a novel probabilistic model, which provides a systematic approach to optimizing EV charging schedules while ensuring grid stability and maximizing renewable energy utilization. Jha et al. [12] examined effective active and reactive power scheduling of Virtual Power Plants while taking phase imbalance and power angle regulation constraints into account. Their work contributes to improving grid stability and efficiency by optimizing power generation and consumption. In [13], the authors proposed a multi-objective optimization approach for charging plug-in EVs in unbalanced distribution networks. This approach addresses the complex interplay between EV charging demands, grid constraints, and multiple optimization objectives, providing valuable insights into achieving sustainable and efficient EV integration. The authors of [14] developed innovative algorithms for optimizing EV charging in microgrid situations, paving the path for more effective and environmentally friendly integration of electric vehicles into the electricity supply. The EV penetration effect with DG is analyzed in [15] for both balanced and unbalanced condition of network. Balu et al. [16] presented an efficient allocation technique for radial distribution systems that include EVCSs and renewable DG with BES. Their research examines the time sequence characteristics of generation and load demand, providing insights into the effective integration of EV charging infrastructure with renewable energy sources to improve grid resilience and sustainability. Ren et al. [17] provided a perspective on the location of EVCSs using the grey decision-making model. Shivashankar et al. [18] provided an overview of various types of overhead transmission line conductors. The paper provides valuable insights into the characteristics, benefits, and applications of various conductor materials used in overhead transmission lines, thereby contributing to a better understanding of modern power transmission technologies. Karmakar et al. [19] presented a new PI controller and artificial neural network controller-based passive cell balancing technique for battery management systems.

Burle et al. [20] presented a modified load flow algorithm that is appropriate for modern power systems operating under fluctuating weather circumstances. Their research overcomes the issues posed by renewable energy integration and weather-related uncertainty. Xu et al. [21] proposed a novel approach for assessing the state of a power system that takes into account transmission line temperature. Temperature data must be incorporated into state estimation models to improve power system monitoring and control accuracy, considering the impact of temperature changes on transmission lines. Haldar et al. [22] undertook a trend examination of long-term meteorological information in a metropolitan area to examine the effects of global weather climate change. They investigate the evolution of climatic trends and their consequences for urban areas. By reviewing historical meteorological data, Albrechtowicz et al. [23] studied how the temperature of overhead transmission lines affects phase-shifting transformer settings. The work focuses on optimizing transformer operations in response to temperature fluctuations along transmission lines using temperature-dependent parameters. Cecchi et al. [24] investigated the impact of temperature fluctuations on transmission line behavior and the implications for power system performance. The authors give a more realistic picture of system dynamics by combining temperature-dependent models into power flow analysis, allowing for improved decisions in grid planning and operation. Dong et al. [25] provided a thorough investigation of power transmission restrictions. The study addresses the issues associated with thermal restrictions in power transfer capacity by examining the electro-thermal coupling in the transmission area. The authors suggest an integrated strategy to accurately assess power transfer limits that take into consideration both electrical and thermal impacts. Burle et al. [26] demonstrate how ambient temperature variations affect the calculation of the vicinity of the voltage collapse point. The study investigates the effect of temperature on voltage stability analysis, an important part of power system performance, taking temperature-dependent characteristics into account. Mishra et al. [27] developed a self-powered temperature monitoring wireless node that uses energy harvesting techniques. The suggested wireless node provides a cost-effective and sustainable solution for temperature sensing in power networks. Rahman et al. [28] presented a comprehensive assessment of research on temperature-dependent analysis of electric power transmission systems. The authors emphasize the need to take temperature impacts into account in system-level research by reviewing a variety of studies. The review covers a variety of topics, including thermal modeling, power flow analysis, and stability evaluation, which provide insight into the intricate interplay between temperature changes and power system behavior. Rakpenthai et al. [29] proposed a study on power system state estimate and line conductor temperature valuation. The authors show that correct temperature estimation is critical for improving the reliability of power system monitoring and control. Koufakis et al. [30] examined the impact of wildfire incidents on transmission line performance, specifically conductor temperature rise, by bringing wildfire dynamics into the modeling framework. Valentina et al. [31] improved the accuracy of power flow analysis and transient stability assessment. The study emphasizes the need to account for temperature changes in transmission line modeling to guarantee that power systems operate reliably and efficiently under a variety of environmental circumstances. Bockarjova et al. [32] studied the significance of temperature changes on the efficacy of state estimation methods, emphasizing the importance of precise temperature measurements in power system monitoring, by assessing the influence of temperature on state estimation accuracy. Du et al. [33] presented an online estimating method for line parameters, temperature, and sag. The authors created a real-time estimation strategy that allows for accurate monitoring of transmission line conditions. Leger et al. [34] presented a flexible method for simulating gearbox line behavior under varied operating conditions. The inclusion of variable parameters allows for a more accurate depiction of transmission line dynamics, which facilitates exact analogue power flow computation. Sagiyeva et al. [35] analyzed the temperature on microstrip lines by examining the effects of temperature changes on microstrip transmission lines; the authors obtained significant insights into the thermal behavior of high-frequency communication

systems. Du et al. [36] worked on building a real-time monitoring method that employs online measurements to reliably estimate transmission line status.

Moghassemi et al. [37] addressed the challenges of grid integration of Photovoltaic (PV) systems and power quality enhancement by incorporating TransZSI-DVR (Trans-Z-source Inverter with Dynamic Voltage Restorer). The authors present an effective solution for minimizing power quality concerns such as voltage sags and harmonics in grid-connected PV systems. Satyanarayana et al. [38] proposed a DC-link fed parallel-VSI DSTATCOM in a solar DG by using DSTATCOM. Oda et al. [39] investigated stochastic optimum planning by integrating photovoltaic-based DG and DSTATCOM while accounting for load and solar irradiance uncertainties. Souza et al. [40] conducted research that sheds light on the complicated dynamics of power injection in DN with PV generation and investigated the relationship between active and reactive power. Albuquerque et al. [41] explored the operation of a PV solar system connected to the electric power grid, acting as both an active power generator and a reactive power compensator. The authors present a comprehensive approach for improving grid stability and power quality. Zubo et al. [42] explored the optimal operation of DN with wind and solar-based energy penetration in a joint both proactive and reactive distribution market. They provide useful insights to grid operators and policy makers, assisting in the development of sustainable energy management policies. Paghdar et al. [43] focused on developing control strategies for distributed generation systems to ensure grid stability and power quality through active and reactive power injection optimization. In the context of climate change, Vincze et al. [44] proposed an inventive ensemble-based experimental investigation on temperature changes. The methodological rigor of this work and its possible consequences for future climate research make it noteworthy. The nonlinear statistical properties of daily temperature changes were investigated by Gyüre et al. [45]. They draw attention to how complex temperature dynamics are and offer a solid framework for understanding how climate systems behave statistically. The approach to select the weightage of objectives for multiple objectives are presented in [46] and the complex multiattribute task based problem is analysed in [47]. The detailed review with concepts related to the solar powered electric vehicle charging system are presented in [48]. The optimal renewable based DG planning in distribution systems considering different objectives and loads effect using distinct optimization techniques are proposed in [49–51]. The tariff bases analysis of hybrid microgrid is explored by [52] to enhance the overall cost economy of the system. In [53], the analysis of potential and policies for photovoltaic electricity generation of the leading countries in solar energy are discovered. The detailed about the battery management system, charging station, traction motors for the electric vehicles are presented in [54]. Three-phase distribution system components planning parameters [55] and analysis related to the renewable DG with EV charging station planning in unbalanced distribution network [55] are reported to find its impact on three phase distribution system. Table 1 illustrates a comparative study of existing works with objective, methodology, research gap, system and findings.

Based on a compressive literature review, it is observed that few authors have considered the balanced and unbalanced distribution system comparative analysis while planning EV charging stations. Also, it was found that the distribution system performance is adversely effected by temperature variation, which is also ignored by the researcher in the distribution system planning. Therefore, the study proposed a comparative analysis of balanced and unbalanced distribution networks with and without EV charging stations considering the sessional temperature variation. Major research articles presented the performance analysis in the balanced IEEE system, but we assume that in practice, some unbalancing load distribution occurs, so our main focus in this paper is to compare the effect, and how to minimize this issue with the unbalancing effect of all three phases separately. This paper explains the unbalancing effect in the balanced case; if unbalancing occurs, then our system knows how to perform and how to improve the voltage, losses, cost-effective factors, and environmental factors.

Table 1. Comparative study of existing works with objective, methodology, research gap, system and findings.

Author (s)	Objective	Methodology/ Optimization	Bus System	Research Gap	Findings
Kathiravan et al. [2]	Minimize line losses by optimally placing EVS	Archimedes Optimization Algorithm (AOA)	IEEE 33	Limited focus on optimization algorithms for minimizing line losses in EVS	The algorithm reduced line losses and improved overall performance
Rajani et al. [3]	Optimize energy management among EV charging stations	GPC-RERNN (Generalized Predictive Control-Recurrent Elman Neural Network)	IEEE 69	Inadequate strategies between EVS	Reducing energy costs and improving grid stability
Ahmad et al. [5]	Optimal deployment of EV fast charging stations with solar DGs	AI approach integrated with reliability analysis	IEEE 33	AI-based solutions that integrate renewable energy sources in EVS	Improved the reliability of the distribution network
Toghranegar et al. [6]	Enhance the hosting capacity for distributed energy resources (DERs)	An optimization technique for load re-phasing	IEEE 37	Limited research on DER hosting capacity in unbalanced networks	Enhanced hosting capacity
Abujubbeh et al. [7]	Probabilistic framework for EVS	Probabilistic framework incorporating spatiotemporal data	IEEE 69	Lack of uncertainty consideration	Provided a robust approach to the planning of uncertainties
Ahmad et al. [9]	Optimal placing solar-powered EVS	Enhanced optimization approach	IEEE 33	Need integration of solar energy in EVS	Effectively integrating solar power and reducing overall network strain
Islam et al. [11]	Correlated EV and grid loads and PV output	Probabilistic model	IEEE 33	Limited research on the correlation between EV, grid loads	Reduced peak loads by effectively coordinating EV charging
Jha et al. [12]	Active and reactive power scheduling in Virtual Power Plants (VPPs)	Multi-objective optimization algorithm	IEEE 37	Need for address phase unbalance in VPPs	Optimized power scheduling, improving VPP efficiency
Esmaili et al. [13]	Optimize the charging of plug-in electric vehicles (PEVs)	PSO	IEEE 13 IEEE 34	Lack of methods addressing the unbalanced nature	Minimized voltage deviations in unbalanced networks
AbuElrub et al. [14]	Charging algorithm for EVs integrated into microgrids with photovoltaic (PV) generation	Heuristic algorithm	IEEE 33	Very less concentration on the integration of EVs with renewable energy sources	EV charging schedules enhancing the utilization of PV
Balu et al. [16]	Allocation of EVS with renewable distributed generation, and battery energy storage	Time-sequence-based optimization	IEEE 69	Need for integrated optimization of EVS and storage systems.	Reduced power losses

Table 1. *Cont.*

Author (s)	Objective	Methodology/ Optimization	Bus System	Research Gap	Findings
Burle et al. [20]	Develop a modified load flow algorithm under variable weather conditions	Modified Newton-Raphson load flow algorithm	IEEE 14 IEEE 33	Need algorithms that can handle variable weather conditions	The algorithm showed improved accuracy under varying weather conditions
Xu et al. [21]	State estimation approach considering transmission line temperature	State estimation	IEEE 14	Limited integration of temperature in state estimation models	Proposed improved the accuracy of state estimation in temperature effects
Cecchi et al. [24]	Examine the system impacts of temperature-dependent transmission line models	Simulation-based analysis	IEEE 30	Limited consideration of temperature effects in traditional transmission line	Demonstrated that temperature-dependent models
Dong et al. [25]	Calculate power transfer limits considering the electro-thermal coupling	Electro-thermal coupling model	IEEE 39	Insufficient integration of electro-thermal effects	Proposed more accurate power transfer limits
Burle et al. [26]	Study the effect of ambient temperature variations	Temperature-dependent voltage collapse analysis	IEEE 118	Lack of studies exploring the direct impact of ambient temperature on voltage stability	Identified that ambient temperature variations significantly influence voltage
Rakpenthai et al. [29]	To estimate power system state and conductor temperature	Joint state and temperature estimation model	IEEE 30	Limited methods for simultaneous state and temperature estimation	Improved estimation in power system state
Valentina et al. [31]	To incorporate temperature variations into transmission line models	Temperature-dependent transmission line model development	IEEE 14	Existing models insufficiently account for temperature variations in transmission line performance	Demonstrated improved accuracy in power flow analysis by incorporating temperature variations
Bockarjova et al. [32]	Impact of transmission line conductor temperature on state estimation accuracy	Temperature-dependent state estimation model	IEEE 30	Lack of detailed analysis on temperature influences state estimation.	Enhances the precision of state estimation
Du et al. [33]	To estimate transmission line parameters, temperature	Online estimation technique using Phasor Measurement Units (PMUs)	IEEE 118	Real-time estimation of temperature and sag	Estimates line parameters, temperature, and sag in real time
Moghassemi et al. [37]	Develop a solar photovoltaic fed TransZSI-DVR	Design and simulation of a TransZSI-DVR system	IEEE 13	Limited research on using TransZSI-DVR systems	Improves power quality, reducing harmonic distortion and voltage sag
Satyanarayana et al. [38]	Solar DG integration	DC-link fed parallel-VSI DSTATCOM	IEEE 33	Lack of robust DSTATCOM solutions for power quality	Improves voltage stability and reduces harmonic distortion

Table 1. *Cont.*

Author (s)	Objective	Methodology/ Optimization	Bus System	Research Gap	Findings
Oda et al. [39]	Integrated PV-based DG and DSTATCOM under load and solar irradiance uncertainties	Stochastic optimization using Monte Carlo simulations.	IEEE 69	Insufficient consideration of uncertainties in PV-based DG and DSTATCOM planning	Improves system reliability and cost-effectiveness by accounting for uncertainties
Souza et al. [40]	Active and reactive power injection in distributed systems	Injection techniques.	IEEE 13	Need for a better understanding of PV system	PV systems can effectively inject both active and reactive powe
Albuquerque et al. [41]	Performance of a PV solar system connected to the grid	Experimental setup with grid-connected PV system	IEEE 33	Limited exploration of dual-functionality PV systems	Enhancing grid reliability
Zubo et al. [42]	To optimize the operation of distribution networks with high wind and solar power penetration	Genetic Algorithm (GA)	IEEE 33	Control strategies in high renewable penetration	Improves network efficiency, reducing power losses
Paghdar et al. [43]	To control active and reactive power in a grid-connected DG	Proportional-Integral (PI) control strategy	IEEE 14	Insufficient focus on control strategies for managing power flow in DG systems	The PI control manages power flow operation under varying load conditions.
Prasad et al. [49]	Perform a cost–benefit analysis for optimal DG placement	Elephant Herding Optimization (EHO)	IEEE 33	Need for cost-effective optimization techniques	Show cost benefit
Rani et al. [50]	Determine the optimal size and placement of renewable DG	PSO algorithm	IEEE 33.	Lack of studies on optimal DG placement considering load variation	Determines optimal DG size and placement, reducing power losses
Bohre et al. [52]	Analyze a grid-connected hybrid microgrid under different utility tariffs	PSO optimization	IEEE 14	Insufficient analysis of hybrid microgrids under varying utility tariffs	Demonstrates impact the economic operation of hybrid microgrids

The proposed work has been analyzed in a three-phase IEEE 69 bus distribution network under day and night global average temperature variation effect in lumped line parameters. This study was performed in different cases and checks the various performances like active and reactive power losses, voltage profile, pollutant emission, and cost of energy loss in both balanced and modified unbalanced load conditions. In this study, four EV corridors and two DG integrations have been integrated to improve performance with the PSO optimization technique. This paper is structured in mainly six different sections with abstract and reference sections. The first section is an introduction, the second section is the modeling of multi-source renewable integrated DG and EV charging stations, the third section is the modeling of a three-phase distributed network, the fourth section is the proposed methodology, the fifth section is the results and discussion and finally, the conclusion, which is the sixth section.

2. Modelling of Multi-Source Renewable Integrated DG and EV Charging Station

2.1. Multi-Source Renewable Integrated DG

Multi-source renewable integrated DG is a hybrid system that can deliver a more steady and dependable power supply; integrating numerous renewable energy sources into a DG system entails mixing various renewable energy technologies (such as biomass, wind turbines, and solar PV). The objective is to maximize grid efficiency and stability while generating, storing, and distributing active and reactive power as efficiently as possible. The modeling and planning of a multi-source renewable integrated distributed generation system are given below.

2.1.1. The Solar Model

The solar PV model, in which active power is based on solar irradiance and temperature, and reactive power in a PV system can be managed using the inverter, which can be controlled to provide or absorb reactive power as needed. The amount of reactive power that can be provided is limited by the inverter's capacity and the amount of active power being generated [48,49].

$$P_{pv} = \eta_{pv} \times A_{pv} \times I \times (1 - \beta(T_{cell} - T_{ref})) \quad (1)$$

where P_{pv} is the power output, η_{pv} is the efficiency, A_{pv} is the area, I is the irradiance, β is the temperature coefficient, T_{cell} is the cell temperature, and T_{ref} is the reference temperature.

The reactive power Q_{pv} provided by the inverter can be calculated as:

$$Q_{pv} = \sqrt{S_i^2 - P_{pv}^2} \quad (2)$$

where S_i represents as inverter capacity that is apparent power in (VA)

2.1.2. The Wind Model

The wind turbine model, wind turbine model, active power based on wind speed, air density, swept area and reactive power can be significant and depends on the type of generator and control strategies [49,50].

$$P_{wind} = 0.5 \times \rho \times A \times v^3 \times \eta_{wind} \quad (3)$$

where P_{wind} is the power output, ρ is air density, A is the swept area, v is the wind speed, and η_{wind} is the efficiency.

2.1.3. The Biomass Model

The biomass model is a model in which active power depends on biomass availability and conversion efficiency and reactive power is produced or consumed depending on the generator type [50–52].

$$P_{biomass} = \eta_{biomass} \times M_{biomass} \times CV \quad (4)$$

$$Q_{bio} = P_{biomass} \times \tan\theta \quad (5)$$

where $P_{biomass}$ and Q_{bio} are the active and reactive power output, $\eta_{biomass}$ is the efficiency, $M_{biomass}$ is the mass flow rate of biomass, and CV is the calorific value.

2.2. Modelling of the EV Charging Station

EV charging stations are critical for accelerating the transition from traditional automobiles to more environmentally friendly and sustainable means of public and private transport. It facilitates grid integration and operation through the development and layout of charging stations, which would have an impact on the electrical system, making it possi-

ble to identify both benefits and potential concerns with grid integration. This involves assessing load control, load ability, and environmental feasibility while using renewable energy to power DN. In this study, two 19.2 kW EV charging stations and two 50 kW loads are integrated according to specifications. Several elements influence the operation of an EV charging station, including the charging station's power rating, the charging protocol, the EV battery's SoC, and any external conditions like temperature or grid demand. Here is a simplified equation that can be used to represent the charging process of an electric vehicle [53,54].

$$P_{ev}(t) = P_{ev\_\max} \times f(t) \times P_{ev}(t) \tag{6}$$

where $P_{ev}(t)$ is the EV power delivered at time t. $P_{ev\_\max}$ is the charging station maximum power rating of EV. $f(t)$ is the charging profile.

DC fast charging is normally controlled by altering the voltage and current supplied by the charger, and (t) may include factors such as battery SoC, temperature, and maximum power constraints. The layout for planning of distribution network with EV and DG is given in Figure 1.

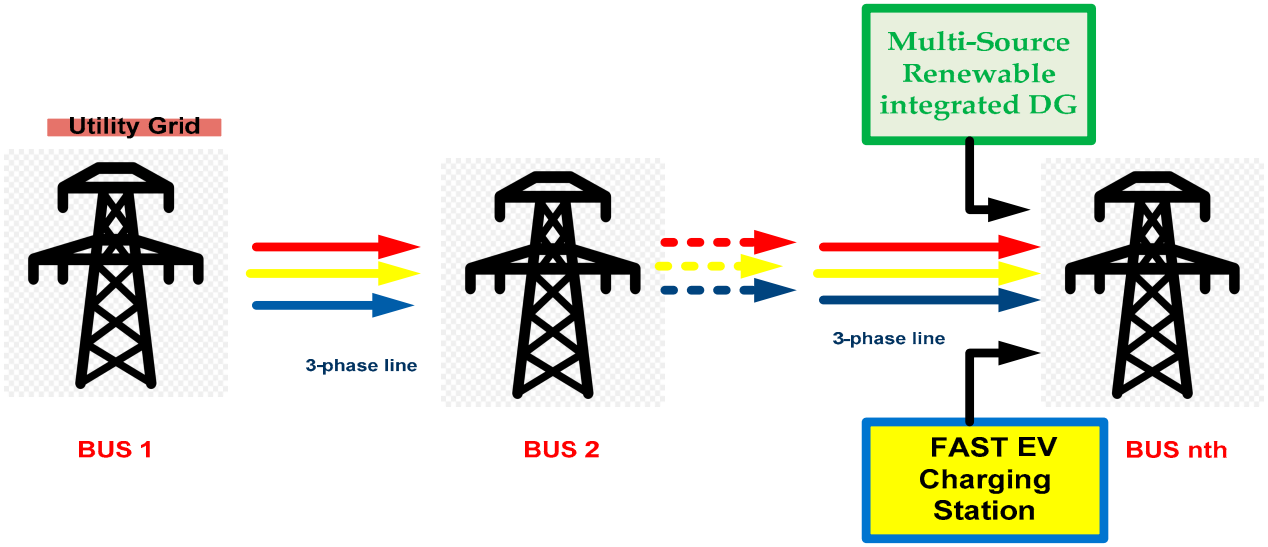

Figure 1. Layout for planning of distribution network with EV and DG.

2.2.1. Modelling the State of Charge (SoC)

It is necessary to comprehend the charging characteristics of the EV battery during fast charging, as well as the charging station's behavior and the charging protocol in use. A simplified formula for simulating the SoC during rapid charging is as follows. Charging and discharging are governed by system conditions and each battery's state of charge [54].

$$SoC(t) = SoC(i) + \int (t_i \times Q_{\max} \times I_{charging}(\tau))\partial\tau \tag{7}$$

where SoC(t) is the state of charge of the battery at time t. $SoC(i)$ is the initial state of charge. $I_{charging}(\tau)$ is the charging current at time t. $Q_{\max}$ is the maximum capacity of the battery. t_i is the initial time of charging. The SoC limits are, $SoC(t)_{\min} \leq SoC(t) \leq SoC(t)_{\max}$

This formula illustrates how the battery's charge builds up over time. The integral term is the entire charge that has been transferred into the battery from the beginning of charging to the present time (t), normalized by the battery's maximum capacity. This is an equation depicting fast-charging SoC behavior; more intricate models may include other variables and dynamics. Table 2 shows the classification of EV charging stations based on different levels, type and locations.

Table 2. Classification of EV charging stations [9,13,15,54].

Classification Criteria	Category	Details	Uses
Charging Power Levels	Level 1 Charging	Voltage: 120 V, Current: Up to 16 A, Power Output: Up to 1.9 kW	Home use with standard outlets
	Level 2 Charging	Voltage: 240 V Current: Up to 80 A (typically 30–40 A), Power Output-Up to 19.2 kW	Home, workplace, public stations
	Level 3 Charging	Voltage: Typically 200–450 V DC, up to 900 V DC, Current: up to 400 A or more, Power Output: 50 kW to 350 kW or more	Public stations along highways
Type of Current	AC Charging	Level 1 and Level 2, In-vehicle Charger: Converts AC to DC for battery charging	Home, workplace, public stations
	DC Charging	Level: Level 3 (DC fast charging)	Public stations along highways, quick charging
Location	Residential	Chargers: Level 1 and Level 2	Home charging, overnight charging
	Public	Chargers: Level 2 and DC Fast Chargers	Parking lots, shopping centers, public places
	Workplace	Chargers: Level 2	Charging during working hours
	Highway/ Corridor	Chargers: DC Fast Chargers	Along highways and major routes
Application	Private Charging	Control: Controlled by individual user	Personal use at home or private spaces
	Commercial Charging	Management: Managed by operators, may require payment	Multiple users in commercial settings
	Fleet Charging	Characteristics: High utilization, multiple charging points, higher power levels	Commercial fleets (e.g., delivery trucks, buses)

The expenditure of EV charging points in the US fluctuates depending on the utilization; Table 3 indicates the costs in USD for level 2, and level 3 [1].

Table 3. Construction and installation cost of different EV charging stations [1].

Type of EV Charging Station	Application	Costs in USD	Source of Report
LEVEL 2	home charging	450–1000	RMI (2017)
LEVEL 2	parking garage	1500–2500	
LEVEL 2	curb side	1500–3000	
LEVEL 3	DC fast EV charging	12,000–30,000	

2.2.2. Fast Charging Station Required Number

The number of fast charging stations in existence is determined by the total amount of electric vehicle load in a given location, as well as the battery capacity used, system load

factor, and EV charging duration. The equation for calculation of approx. EV charging station number is given in [4].

$$N_{FCS}^{ev} = \frac{P_{ev} \times n_{ev} \times C_{time}}{C_{st} \times C_{\eta} \times L_F \times N_c \times p.f} \tag{8}$$

where P_{ev} denotes the total average power of EV, n_{ev} represents the number of EV, C_{time} is the charging time per day, C_{st} denotes the charger service time, C_{η} denotes charging efficiency, the load factor $L_F \times N_c$ is for the number of connectors in FCS, and $p.f$ denotes the power factors.

3. Modelling of the Three-Phase Distributed Network

Three-phase balanced and unbalanced systems are characterized by symmetrical components; however, in this work, the phase frame approach [55] of three-phase load flow is used to easily analyze the system. In the current system, mesh and node analysis for load flow should be performed. IEEE 69 bus mesh and nodal analysis have been used to account for three-phase balancing and unbalanced load flow. The phase frame approach is used to achieve three-phase balanced and unbalanced system performance [55,56]. Let us examine a simple three-phase lumped network diagram represented in Figure 2. The variables considered in Figure 2 represented for m node system with three phases a, b, c. Also $R_{L1a}, R_{L1b}, R_{L1c}$, $X_{L1a}, X_{L1b}, X_{L1c}$, $Z_{1a\_s}, Z_{1b\_s}, Z_{1c\_s}$ are the self resistances, self reactances and self impedances of lines for three phases a, b, c respectively. Similarly, the mutual impedance for the distributed network are $Z_{12\_m}, Z_{12\_m}, Z_{13\_m}$ can aslo be represented with its respective parameters for system..

$$\begin{bmatrix} v_1^a \\ v_1^b \\ v_1^c \\ v_1^n \end{bmatrix} - \begin{bmatrix} v_2^a \\ v_2^b \\ v_2^c \\ v_2^n \end{bmatrix} = \begin{bmatrix} z_{11\_s} & z_{12\_m} & z_{13\_m} & z_{1n\_m} \\ z_{21\_m} & z_{22\_s} & z_{23\_m} & z_{2n\_m} \\ z_{31\_m} & z_{32\_m} & z_{33\_s} & z_{cn\_m} \\ z_{n1\_m} & z_{n2\_m} & z_{n3\_m} & z_{nn\_s} \end{bmatrix} \begin{bmatrix} i_{12}^a \\ i_{12}^b \\ i_{12}^c \\ i_{12}^n \end{bmatrix} \tag{9}$$

where $z_{11\_s}, z_{22\_s}, z_{33\_s}$ is the self-impedance and $Z_{12\_m}, Z_{12\_m}, Z_{13\_m}$ is the mutual impedance for the distributed network.

$$v_{branch} = v_1^{abcn} - v_2^{abcn} = z^{abcn} \times i^{abcn} \tag{10}$$

where the branch voltage v_{branch}, the branch current i^{abcn}, and the primitive impedance matrix z^{abcn} are set in the distribution system.

$$Y^{abcn} = (Z^{abcn})^{-1} \tag{11}$$

where Y^{abcn} is the primitive admittance matrix.

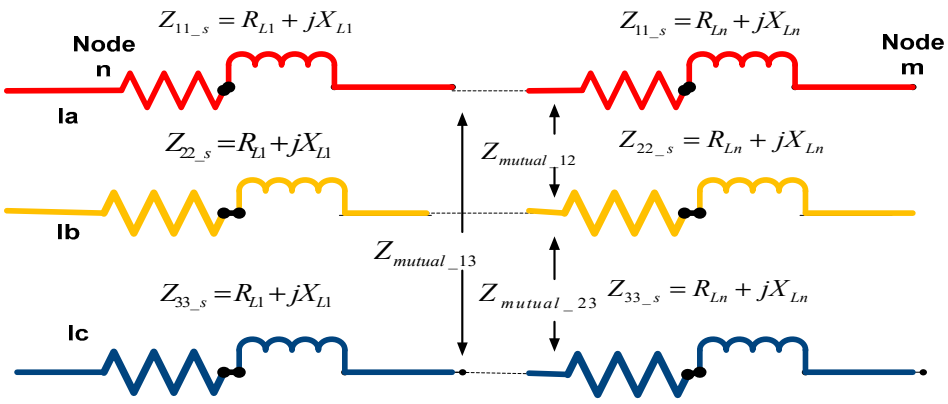

Figure 2. The three-phase distributed network.

All primary and secondary windings' admittance as well as their per unit value are considered in this analysis. In the balanced case study, all transformer topologies were star wound. However, the unbalanced case study additionally included some delta configurations. Therefore, the admittance matrix must be generated for conversion. Leakage admittance has not been taken factored into the load flow estimations of the current study. A power system that highlights fluctuating voltages as a result of different phase angles or unbalanced voltage values is known as an unbalanced DN. Figure 3 illustrates the representation of EV corridors in the single-line diagram of the IEEE 69 bus network.

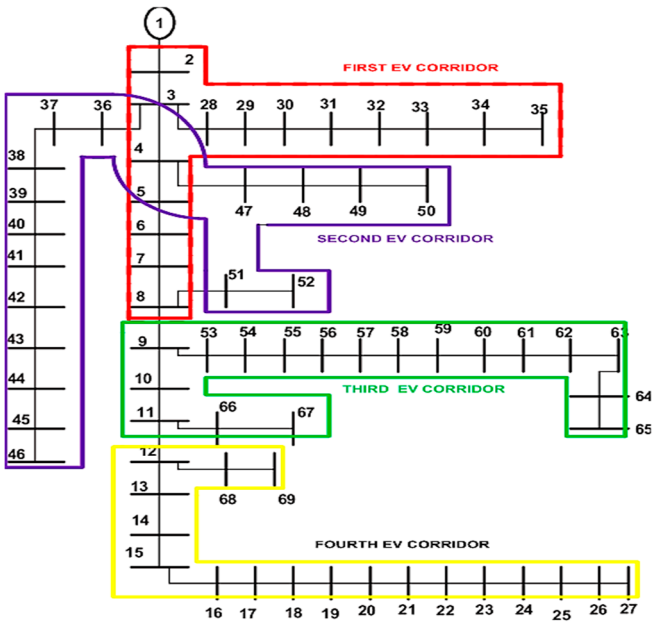

Figure 3. Single-line diagram of the IEEE 69 bus network with EV corridors representation.

The Modelling Effect on Distribution Due to the Temperature Effect

In the radial distribution model uniformly distributed series resistance, series inductance is defined in per unit length [35]. In this model, temperature is assumed to be a constant parameter, but nowadays, many power electronic static devices are connected to the system, and in static devices, temperature can affect performance. So, in this study, temperature effects are considered for further load flow analysis [20–24].

$$R^{line}_{T_{actual}} = R^{line}_{T_{ref}}(1 + \alpha(T_{actual} - T_{ref}) \tag{12}$$

where

T_{ref} is the reference 20 degree temperature [33],
T is the radial line actual sessional global temperature,
$R^{line}_{T_{ref}}$ is the radial line resistance at reference in ohms,
$R^{line}_{T_{actual}}$ is the radial line resistance at sessional temperature in ohms, and
α is the resistance temperature coefficient, considered as 0.0033/°C [33].

$$X^{line}_{\omega,T_{actual}} = X^{line}_{\omega,T_{ref}}(1 + \beta(T_{actual} - T_{ref}) \tag{13}$$

where $X^{line}_{\omega,T_{ref}}$ is the radial line reactance at reference temperature in ohms, $X^{line}_{\omega,T_{actual}}$ is the radial line reactance at sessional temperature in ohms, ω is the angular network frequency, β is the reactance temperature coefficient [24] of the ACSR conductor, i.e., β = 0.00429 in/°C [20].

The steady-state current flowing through the radial conductor can be calculated by the heat balance equation

$$i_{current}^{eff} = \sqrt{\frac{(q_{con} + q_{rad} + q_{sol})}{R_T^{line}}} \quad (14)$$

where $i_{current}^{eff}$ is the effective current flowing in the radial line, $q_{con}, q_{rad}, q_{sol}$ are the heat losses by convection, radiation and solar heat consumed by the conductor, and the formulas for calculation are mentioned in IEEE standard 738-2006 [29].

This study examines four cases of temperature change, varying the transmission line bus parameters in a sessional and day–night manner. A temperature reference of 20 °C is used while developing standard resistance and inductance. For the case study, the average annual night temperature was 18 °C, while the average annual day temperature was 32.33 °C. The details about the seasonal temperature are mentioned in Table 4.

Table 4. Monthly averaged weather data of India [20].

Month	Day Temperature in °C	Night Temperature in °C	Sessional Weather	Avg. Day Temp °C	Avg. Night Temp °C
Dec	23	7	Winter	23.33	7.83
Jan	23	6.5			
Feb	24	10			
Mar	32	14	Summer	37.33	19.66
Apr	37	20			
May	43	25			
Jun	38	29	Monsoon	36.33	26.66
Jul	36	26			
Aug	35	25			
Sep	35	23	Post-monsoon	32.33	18
Oct	35	19			
Nov	27	12			

4. Proposed Methodology

The backward–forward load flow method was adopted for the distribution network, and the backward–forward load flow analysis of the IEEE 69 bus, encompassing both unbalanced and balanced loads, was performed with the aid of KVL and KCL.

4.1. Multi-Objective Function (MOFs)

Multi-objective functions are widely used in complex scenarios that require balancing many objectives throughout the decision-making phase. MOFs allow for the optimized performance of conditions with numerous objectives. This analysis takes into account characteristics such as minimal voltage variation, minimal phase angle variation, and both reactive and active power losses.

$$MOF = k_a \times API_{loss\_index} + k_b \times V.D.I_{index} + k_c \times RPI_{loss\_index} \quad (15)$$

where k_a, k_b, k_c are the priority-based performance index weightage coefficients. The weight factor in this work is determined using the weighted sum approach [46], which adds up all of the specified weighted objectives to create a composite objective whose sum equals unity. The analytic hierarchy process approach is used to generate the weight indexing coefficient for each objective [47]. Here, the equation for the priority matrix (P) is provided, with details given in Table 5.

$$P = \begin{bmatrix} 1 & 3 & 2 \\ 1/3 & 1 & 1/5 \\ 1/2 & 5 & 1 \end{bmatrix}$$

Table 5. The pairwise comparison matrix.

Parameters	Active Power Losses	Voltage Deviation	Reactive Power Losses
Active power losses	1	3	2
Voltage deviation	1/3	1	1/5
Reactive power losses	1/2	5	1

Where 1—equal priority, 3—moderate, 5—strong, 7—very strong, 9—extreme and 2, 4, 6, and 8—intermediate priority.

The weight factors that were calculated by the analytic hierarchy process approach are 0.5012, 0.1185, and 0.3803; these are used in the objective function as the indexing coefficients for k_a, k_b, and k_c.

The formulation of the distribution system performance index is as follows:

The Active Power Losses Index (API_{loss_index})

$$API_{loss\_index} = \frac{P^{Phase\_a}_{loss_{with\_DG,EV}} + P^{Phase\_b}_{loss_{with\_DG,EV}} + P^{Phase\_c}_{loss_{with\_DG,EV}}}{P^{Phase\_a}_{loss_{base}} + P^{Phase\_b}_{loss_{base}} + P^{Phase\_c}_{loss_{base}}} \quad (16)$$

The Reactive Power Losses Index (RPI_{loss_index})

$$RPI_{loss\_index} = \frac{Q^{Phase\_a}_{loss_{with\_DG,EV}} + Q^{Phase\_b}_{loss_{with\_DG,EV}} + Q^{Phase\_c}_{loss_{with\_DG,EV}}}{Q^{Phase\_a}_{loss_{base}} + Q^{Phase\_b}_{loss_{base}} + Q^{Phase\_c}_{loss_{base}}} \quad (17)$$

The Voltage Deviation Index (VDI)

$$V.D.I_{index} = Maximum\left(\frac{V_{phase\_a} - V_{ref}}{V_{ref}} + \frac{V_{phase\_b} - V_{ref}}{V_{ref}} + \frac{V_{phase\_c} - V_{ref}}{V_{ref}}\right) \quad (18)$$

where 1.0 pu is considered as V_{ref}.

The details about the bus location in EV corridors in the IEEE69 bus network are given in Table 6 with the EV corridors bus location, type, size and cost information to plan for the different EV charging stations in the respective EV corridors.

4.2. Substation Power Supply Cost

The cost of supplying a grid substation is divided into various components, reflecting the complexity and scope of the infrastructure required to properly manage and distribute electricity. Here is a breakdown of the primary cost components connected with grid substation supply [50]:

$$\text{Cost}_{sub\_station} = c_s \times \sqrt{(P_s^2 + Q_s^2)} \quad (19)$$

where P_s, Q_s are the active and reactive power supply by grid.

4.3. Cost of Energy Loss (Per Annum)

An electrical distribution system's overall operational efficiency and expenses, particularly those of grid substations, are significantly influenced by energy loss costs. When determining the annual cost of energy loss, it is vital to take into account the total energy

provided to the distribution system year over year, the percentage of energy lost due to resistance in transmission lines and transformers, and the cost of power per unit [49].

$$CEL_{per\_year} = P_{total\_loss} \times (k_{cp}R_L + k_{ep}R_L + LF \times 8760) \quad (20)$$

$$Loss\ factor(LF) = R_b \times lf + (1 - R_b) \times lf^2 \quad (21)$$

where R_b is taken as 0.2, 0.47 is the load factor, k_{cp} is 57.6923 USD/kw for this test study, and k_{ep} to plan for taken as 0.00961538 USD/kwh [49].

Table 6. Details about the bus location in EV corridors in the IEEE69 bus network.

Corridor Name	BUS No.	Type of EV Charging	Application	Size of EV (kW)	Costs in USD [1]
First EV Corridor	2, 3, 4, 5, 6, 7,8, 28, 29, 30, 31, 32, 33, 34, 35	LEVEL 2	Home, workplace, public stations	19.2	450–1000
Second EV Corridor	36, 37, 38, 39, 40, 41, 42, 43, 44, 45, 46, 47, 48, 49, 50, 51, 52	LEVEL 2	Home, workplace, public stations	19.2	450–1000
Third EV Corridor	9, 10, 11, 53, 54, 55, 56, 57, 58, 59, 60, 61, 62, 63, 64, 65, 66, 67	LEVEL 3	DC fast EV charging (public stations along highways)	50	12,000–30,000
Fourth EV Corridor	12, 13, 14, 15, 16, 17, 18, 19, 20, 21, 22, 23, 24, 25, 26, 27, 68, 69	LEVEL 3	DC fast EV charging (public stations along highways)	50	12,000–30,000

4.4. Distributed Generation (DG) Cost

DG is the decentralized production of energy close to the point of demand rather than at a big, central facility. DG systems include solar PV, wind turbines, small-scale hydro, biomass, fuel cells, and diesel generators. The cost of supplying power via DG varies according to the type of generation technology used [49,50]. Equations (22) and (23) represent the active and reactive power cost function.

$$C_{P_{DG}} = g_1 \times P_{DG}^2 + g_2 \times P_{DG} + g_3 \quad (22)$$

where $C_{P_{DG}}$ is the active power cost and $C_{Q_{DG}}$ is the reactive power cost.

$$C_{Q_{DG}} = [cost(\frac{1.1 \times P_{DG}}{pf}) - cost(\sqrt{((\frac{1.1 \times P_{DG}}{pf})^2 - Q_{DG}^2)}] \times c_k \quad (23)$$

where the coefficients are considered as $g_1 = 0$, $g_2 = 20$, $g_3 = 0.25$ and $c_k = 0.05$–0.1.

4.5. Greenhouse Gas Emissions

Greenhouse gases (GHGs) are gases found in the atmosphere which cause global warming and the greenhouse effect. It is imperative to reduce greenhouse gas emissions in order to mitigate the effects of global warming on ecosystems and human societies. In order to combat climate change and advance a sustainable future, greenhouse gas emissions must be reduced. The pollutant emission factor for CO_2 is 632.0 g/kWh, whereas that for SO_2 is 2.74 g/kWh and that for NOx is 1.34 g/kWh [52]. The typical greenhouse gas emission calculation formula is [54].

$$G_{emission} = E_{grid} \times G_{em-factor} \times (1 - G_{re-efficency}) \quad (24)$$

where $G_{re-efficency}$ is the overall greenhouse reduction efficiency, $G_{em-factor}$ is the greenhouse emission factor (g/kWh), and E_{grid} represents the entire substation power capacity in (kWh).

4.6. Constraints

Power system constraints and limitations are essential elements that need to be taken into account during planning and operation to ensure effective, reliable, and stable power. To maintain system stability, power system design requires certain limitations. Limits need to be defined for voltage limits, active and reactive power demand, power balance, and the number of EV charging stations [4].

$$\begin{gathered} v_i^{\min} \leq v_{bus} \leq v_i^{\max} \\ P_{dg}^{\min} \leq P_{dg} \leq P_{dg}^{\min} \\ Q_{dg}^{\min} \leq Q_{dg} \leq Q_{dg}^{\min} \\ P_{EV} + P_{Distrubution\_load} = P_{DG} + P_{Grid} \\ N_{ECS}^{\min} \leq N_{ECS} \end{gathered}$$

4.7. Particle Swarm Optimization

The PSO originated from a social interaction that resulted from the combination of biological mobility and swarm intelligence behavior. The PSO developer looks for the ideal place to gather food for the group as well as for individuals while travelling in a swarm. Each particle in the swarm is separately represented by the vector x(t) and velocity v(t). Each particle in the swarm uses its individual experience to guide it towards the food. Swarms follow each other as they look for the optimal spot. To update location and velocity in the direction of the food hunt, the swarm optimizes in two stages: locally best first, and then group global best [51].

$$Y_{i=n}^{n+1} = k_p \times (a_1 \times r_1 \times (G_{best} - Y_{i=n}^{n}) + a_2 \times r_2 \times (G_{best} - Y_{i=n}^{n})) \tag{25}$$

where r_1, r_2 are random variables with values ranging from 0 to 1 and k_p is the PSO weight factor, a_1, a_2 are PSO acceleration coefficients. Figures 4 and 5 show the flow chart of the proposed methodology and PSO the optimization flow chart, respectively.

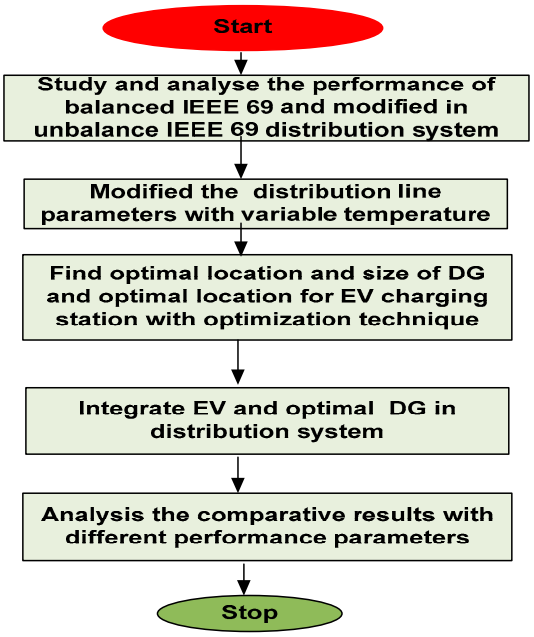

Figure 4. Flow chart of the proposed methodology.

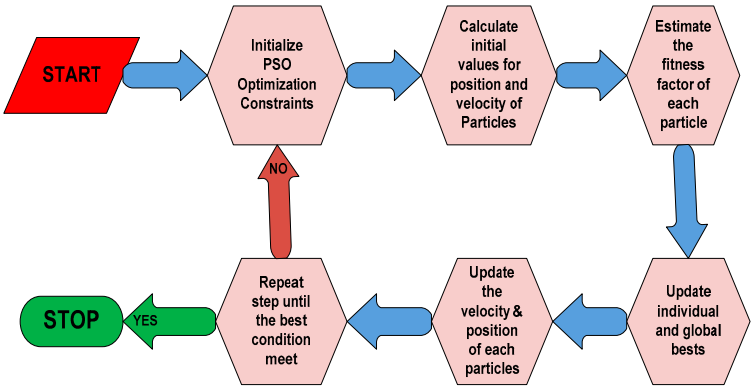

Figure 5. PSO optimization flow chart.

5. Results and Discussion

A three-phase IEEE 69 bus network has been taken as a reference to analyze the implemented work parameters for this comparative study. The data of IEEE 69 bus three phase balanced and modified unbalanced system is given in Appendix A. In the distribution network, due to the large R/X ratio, the three-phase backward–forward load flow sweep method is used to compute the three-phase balanced and modified unbalanced system. In this study, temperature-dependent effected parameters are considered in three cases. In Case I, all the performance parameters are computed in standard reference temperature. In Case II, the average night temperature of 18 °C is considered, and in Case III, the average day temperature of 32.33 °C is considered to analyze the line parameters effect for different seasons. In all the cases, DG and four mixed-level EV corridors integrated to improve the performance as well as economics and environmental factors. To maximize the objective benefit, DG and EV location in optimal place and size with the help of PSO optimization technique. All three cases perform in both balanced and modified unbalanced networks with the same objective, and performance parameters have been measured for discussion in this work.

The optimal size and location of DG and EV were computed with the help of PSO, which is tabulated in Tables 7 and 8 in all three considered cases. In both the balanced and unbalanced bus systems, DG 2 is located at bus no 50 in all cases, but DG1's optimal location changes in all cases as per tabular data. The EV1 and EV2 are located in the first and second corridors, and their size is 19.2 kW, but EV3 and EV4 are located in the third and fourth corridors with a size of 50 kW. The minimum, maximum value of voltage and the average voltage deviation for balanced and unbalanced networks are given in Tables 9 and 10.

Table 7. DG and EV size and location in IEEE-69 balanced network.

IEEE 69 BAL-ANCE	Case I			Case II			Case III		
	Size		Bus Location	Size		Bus Location	Size		Bus Location
	P (kW)	Q (kW)		P (kW)	Q (kW)		P (kW)	Q (kW)	
DG1	655.74	262.384	18	657.03	406.64	15	499.78	410.69	16
DG2	1721.44	1150	50	1850	1137.81	50	1850	1150	50
	EV SIZE (kW)	EV LEVEL		EV SIZE (kW)	EV TYPE		EV SIZE (kW)	EV TYPE	
EV1	19.2	LEVEL 2	35	19.2	LEVEL 2	2	19.2	LEVEL 2	5
EV2	19.2	LEVEL 2	38	19.2	LEVEL 2	49	19.2	LEVEL 2	52
EV3	50	LEVEL 3	10	50	LEVEL 3	60	50	LEVEL 3	64
EV4	50	LEVEL 3	24	50	LEVEL 3	69	50	LEVEL 3	20

Table 8. DG and EV size and location in the modified IEEE-69 unbalanced network.

Modified IEEE 69 Unbalance	Case I			Case II			Case III		
	Size		Bus Location	Size		Bus Location	Size		Bus Location
	P (kW)	Q (kVAr)		P (kW)	Q (kVAr)		P (kW)	Q (kVAr)	
DG1	520.41642	434.3319	17	493.1669	377.1205	17	577.1405	407.9346	16
DG2	1703.1085	1150	50	1850	1150	50	1850	1150	50
----	EV SIZE (kW)	EV LEVEL		EV SIZE	EV TYPE	LOCATION	EV SIZE (kW)	EV TYPE	-----
EV1	19.2	LEVEL 2	2	19.2	LEVEL 2	29	19.2	LEVEL 2	30
EV2	19.2	LEVEL 2	52	19.2	LEVEL 2	36	19.2	LEVEL 2	44
EV3	50	LEVEL 3	56	50	LEVEL 3	59	50	LEVEL 3	55
EV4	50	LEVEL 3	23	50	LEVEL 3	18	50	LEVEL 3	18

Table 9. Minimum, maximum voltage and average deviation in the balanced network.

Modified IEEE 69 Balance	Case I		Case II		Case III	
	Without DG and EV	With DG and EV	Without DG and EV	With DG and EV	Without DG and EV	With DG and EV
Minimum voltage Deviation	Phase A/ Phase B/ Phase C	0.82497	0.96052	0.88291	0.97376	0.82497	0.96052
Maximum voltage Deviation	Phase A/ Phase B/ Phase C	1	1.00049	1	1.0043	1	1.00001
Average voltage	Phase A/ Phase B/ Phase C	0.97337	0.99783	0.97466	0.9996	0.96403	0.99706

Table 10. Minimum, maximum voltage and average deviation in the unbalanced network.

Modified IEEE 69 Unbalance		Case I		Case II		Case III	
		Without DG and EV	With DG and EV	Without DG and EV	With DG and EV	Without DG and EV	With DG and EV
Minimum voltage Deviation	Phase A	0.87662	0.96641	0.88291	0.97376	0.82497	0.96052
	Phase B	0.92389	0.99528	0.92756	0.99629	0.89514	0.99563
	Phase C	0.92511	0.98724	0.92872	0.98792	0.89699	0.98443
Maximum voltage Deviation	Phase A	1.00000	1.00000	1.00000	1.00000	1.00000	1.00244
	Phase B	1.00000	1.00734	1.00000	1.01239	1.00000	1.01544
	Phase C	1.00000	1.00835	1.00000	1.01334	1.00000	1.01686
Average voltage	Phase A	0.96885	0.99333	0.97041	1.00094	0.95736	0.99325
	Phase B	0.97714	1.00005	0.97823	0.99785	0.96923	1.00178
	Phase C	0.97372	0.99682	0.97497	1.00094	0.96456	0.99748

The voltage profiles for every case are displayed in Figures 6–11. In Figures 6–8, all three cases are evaluated in balance load data, but at the same time, Figures 9–11 show the modified unbalanced load data in all three phases, the magnitude of minimum, maximum, and average voltage deviation voltage is tabulated in Tables 9 and 10. The minimum voltage found in Case III, in unbalanced case phase A, is 0.82497 pu without DG and

EV integration, but after integration, it improves. The maximum voltage is 1.00244 pu in unbalanced case phase A after the DG and EV integration. In all the cases, per-phase voltage improves after the DG and EV integration.

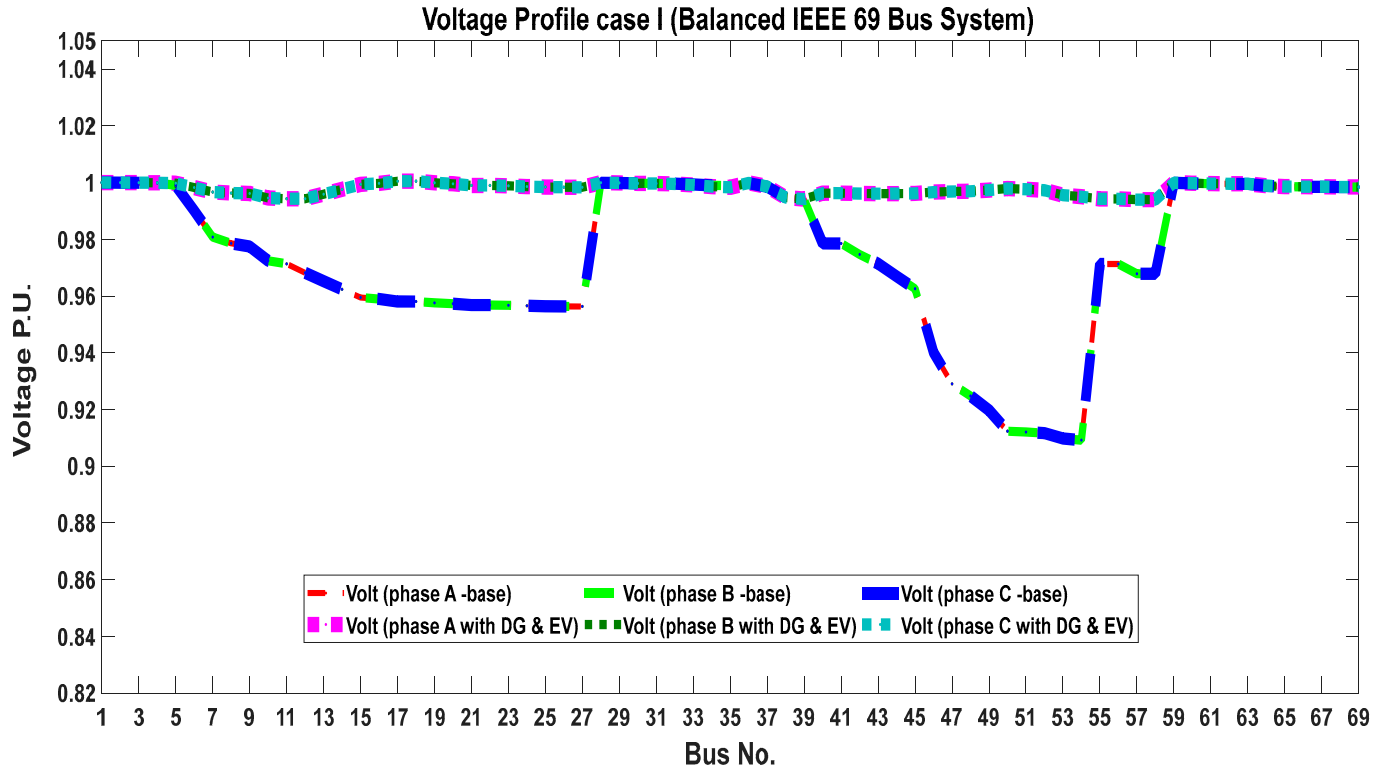

Figure 6. Voltage profile for Case I (per phase) in the balanced load case.

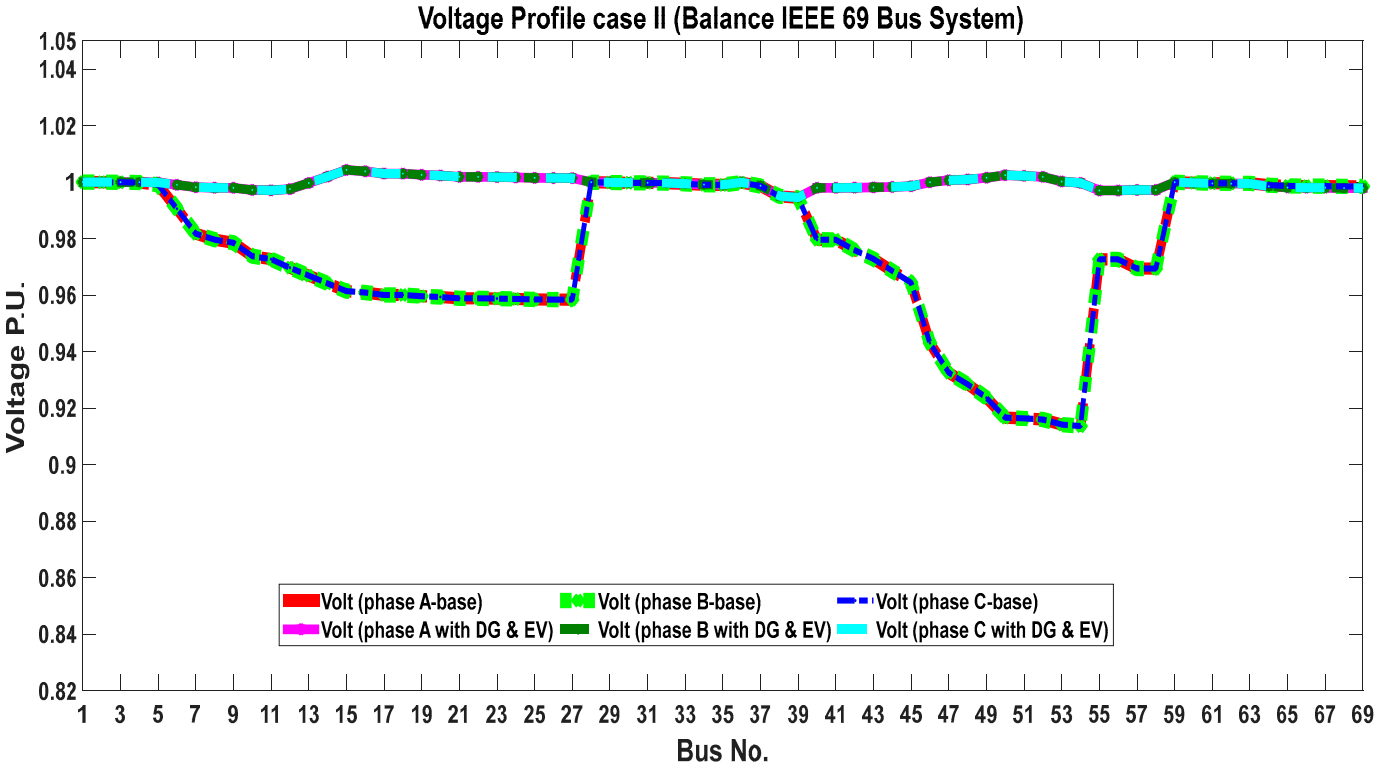

Figure 7. Voltage profile for Case II (per phase) in the balanced load case.

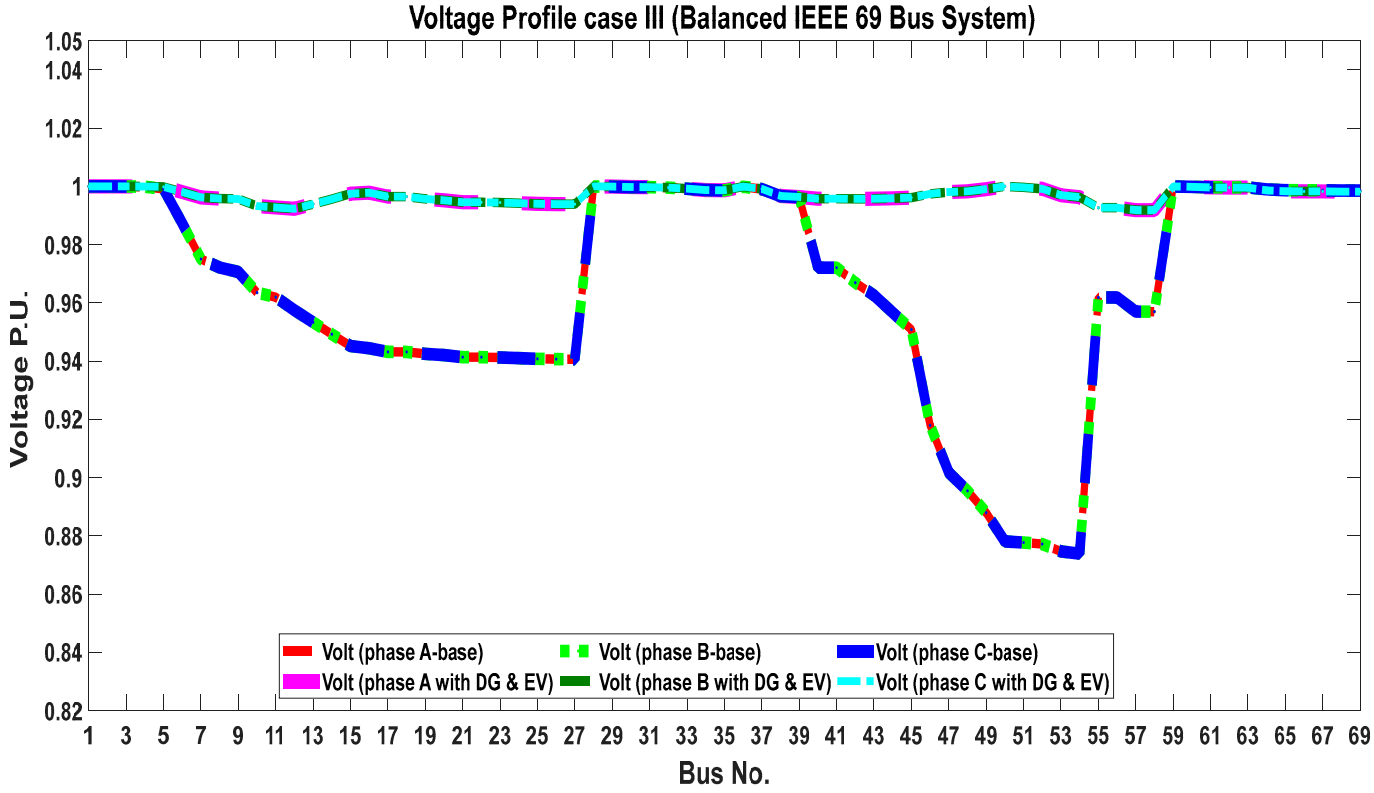

Figure 8. Voltage profile for Case III (per phase) in the balanced load case.

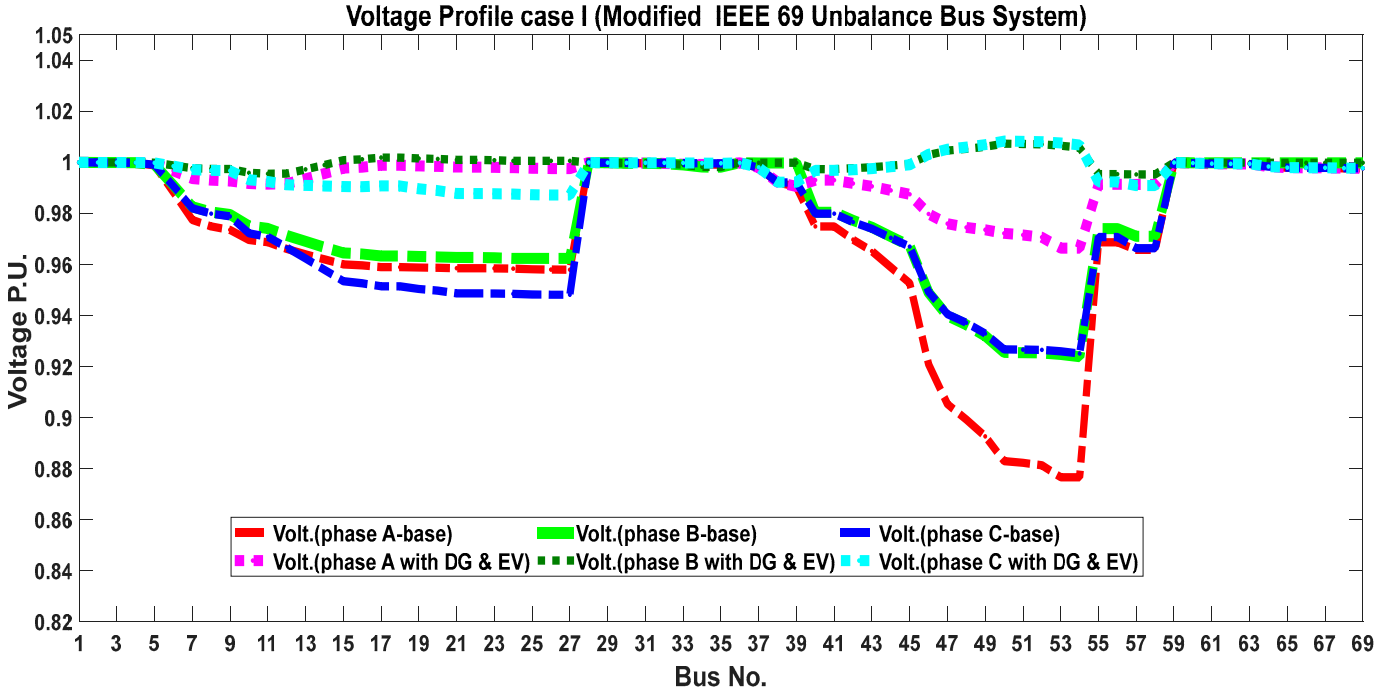

Figure 9. Voltage profile for Case I (per phase) in the unbalanced load case.

Table 11 shows the economics analysis for the CEL and DG installation cost estimated in all the cases and conditions. In the balanced case, DG costs are 29,370.13, 32,116.41, 32,454 USD, and in the unbalanced case, these are 32,945.71, 31,756.02, 32,454 USD in case I, case II, and case III. The CEL savings after DG and EV integration increased by 95.96, 96.01, 96.05 percent in balance and 91.79%, 92.06%, 92.46% in unbalanced cases.

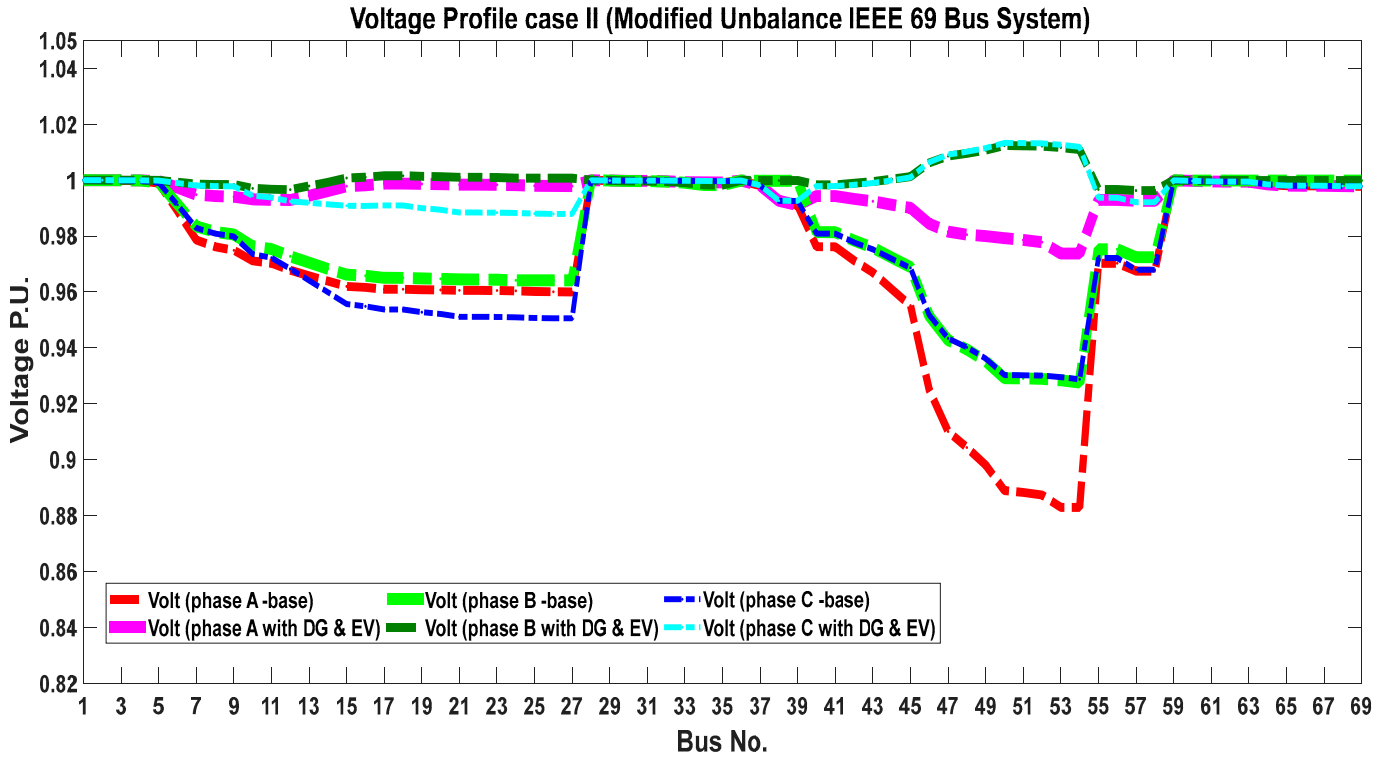

Figure 10. Voltage profile for Case II (per phase) in the unbalanced load case.

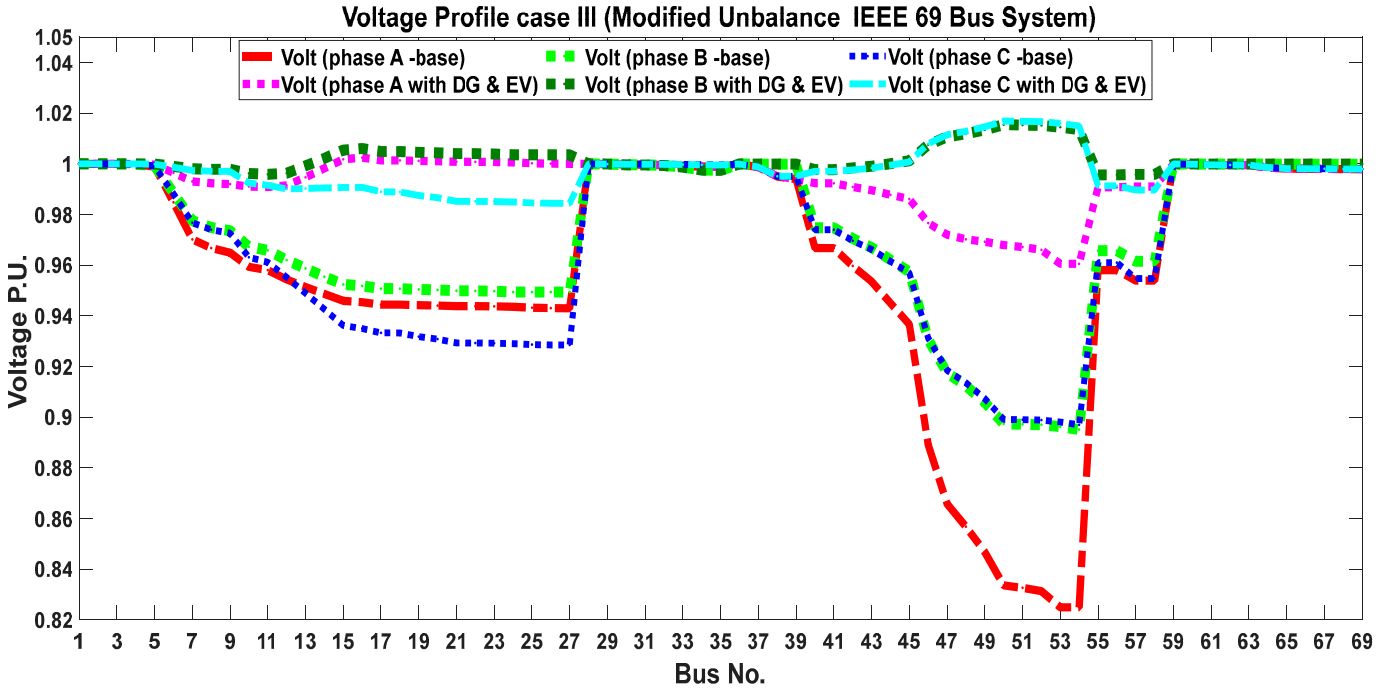

Figure 11. Voltage profile for Case III (per phase) in the unbalanced load case.

In this study, active and reactive power loss reduction is the prime objective with the integration of both DG and EV; here, a three-phase analysis has been performed to find out all per-phase branch losses. In balance bus condition, active losses are 225.03 kW, 213.824 kW, and 250.337 kW in case I, case II, and case III, and the reactive power losses are 102.116 kVAr,95.046 kVAr, 238.961 kVAr. Then, after DG and EV, its losses were reduced. Modified three-phase unbalanced case active and reactive power loss data are tabulated

in Tables 12 and 13. Here, due to unbalanced load distribution in the three phases, the system becomes more nonlinear; thus, active and reactive loss increases compared to the balanced case. When computing the loss without DG and EV, the total active power losses are 242.698 kW, 230.111 kW, 273.857 kW, and total reactive power losses are 112.066 kVAr, 105.031 kVAr, 261.413 kVAr in three cases, respectively. But after DG and EV integration in optimal location and size losses decrease in all the case scenarios, individual per phase active and reactive loss data are tabulated in Tables 12 and 13.

Table 11. CEL, DG cost in the IEEE-69 balanced network and the modified IEEE-69 unbalanced network.

Economic Factor	IEEE 69 Bus Network				Modified IEEE 69 Unbalance Bus Network			
	DG COST(USD)	CEL(USD)_Without DG and EV	CEL(USD)_With DG and EV	CEL Saving in %	DG COST(USD)	CEL(USD)_Without DG and EV	CEL(USD)_With DG and EV	CEL Saving in %
Case I	29,370.13	18,111.65	730.95	95.96%	32,945.71	19,536.04	1604.09	91.79%
Case II	32,116.41	17,211.83	686.89	96.01%	31,756.02	18,538.92	1472.32	92.06%
Case III	32,454.00	20,150.92	706.16	96.50%	32,454.00	22,044.15	1662.38	92.46%

Table 12. Active and reactive power loss in IEEE-69 balanced network.

IEEE 69 Balance Network		Case I		Case II		Case III	
		Without DG and EV	With DG and EV	Without DG and EV	With DG and EV	Without DG and EV	With DG and EV
Active power loss (kW)	Phase A	75.001	3.027	71.275	2.844	83.446	2.924
	Phase B	75.001	3.027	71.275	2.844	83.446	2.924
	Phase C	75.001	3.027	71.275	2.844	83.446	2.924
	Total	225.003	9.081	213.824	8.533	250.337	8.773
Reactive power loss (kVAr)	Phase A	34.055	3.015	31.955	2.732	79.654	2.791
	Phase B	34.055	3.015	31.955	2.732	79.654	2.791
	Phase C	34.055	3.015	31.955	2.732	79.654	2.791
	Total	102.166	9.046	95.864	8.197	238.961	8.374

Table 13. Active and reactive power loss in the modified IEEE-69 unbalanced network.

Modified IEEE 69 Unbalance		Case I		Case II		Case III	
		Without DG and EV	With DG and EV	Without DG and EV	With DG and EV	Without DG and EV	With DG and EV
Active power loss (kW)	Phase A	128.146	12.173	121.262	9.217	148.325	10.550
	Phase B	54.165	2.448	51.553	3.004	59.449	3.562
	Phase C	60.388	5.307	57.496	6.070	66.082	6.540
	Total	242.698	19.928	230.311	18.291	273.857	20.652
Reactive power loss (kVAr)	Phase A	58.758	9.472	54.925	7.958	141.585	10.071
	Phase B	23.697	0.949	22.262	1.143	56.748	3.400
	Phase C	29.611	5.577	27.844	5.622	63.079	6.243
	Total	112.066	15.998	105.031	14.724	261.413	19.713

The emission of harmful greenhouse gas parameters is also reduced in this case study, which is tabulated in Table 14. Here, CO_2, SO_2, NO_x, and CO gas are considered for calculation as per Equation (24). The total emission of greenhouse gases is 632.468 g/kWh, and their effect is calculated with and without DG and EV cases in both balanced and

unbalanced conditions. In the balanced case, the emission was reduced by 61.4%, 64.5%, and 60.98% in all three study cases, and in the modified unbalanced condition, it was reduced by 57.55%, 60.39%, and 62.79%. Table 15 shows the comparative analysis of grid supply efficiency in balanced and unbalanced networks in all cases. The results analysis shows that the efficiency has increased while considering the DG and EV planning in the distribution network. The total power losses and efficiency for different cases of the balanced system for the case I at standard temperature are 247.1118 MVA and 95.27% (without DG and EV) and 12.81775 MVA and 99.71% (with DG and EV), for case II at 18 °C temperature are 234.3301 MVA and 95.51% (without DG and EV) and 11.83228 MVA and 99.73% (with DG and EV) and for case III at 32.33 °C temperature are 346.0794 MVA and 92.75% (without DG and EV) and 12.12804 MVA and 99.70% (with DG and EV), respectively. Similarly, for the different cases of the unbalanced system the total power losses and efficiency for the case I at standard temperature are 267.3221 MVA and 94.34% (without DG and EV) and 25.55506 MVA and 99.46% (with DG and EV), for case II at 18 °C temperature are 253.1297 MVA and 94.62% (without DG and EV) and 23.48099 MVA and 99.51% (with DG and EV) and for case III at 32.33 °C temperature are 378.5953 MVA and 92.79% (without DG and EV) and 28.55009 MVA and 99.42% (with DG and EV) correspondingly. This analysis clearly shows that the losses are increased, and the efficiency is reduced with the increment in the temperature for the balanced and unbalanced systems. Here, it is clearly found that the unbalanced nature will also affect system performance by temperature variations. As shown in the analysis, the losses are always high and the efficiency is low for the unbalanced system as compared to the balanced system.

Table 14. Emission factor calculation.

Emission Factor	Emission of Greenhouse Gases in g/kWh				Emission of Greenhouse Gas in g/kWh	Greenhouse Gas Yearly in Tonnes without DG	Greenhouse Gas Yearly in Tonnes after DG	Emission Saving after Renewable DG
	IEEE 69 Balanced Case							
	CO_2 (g/kWh)	SO_2 (g/kWh)	NO_x (g/kWh)	CO (g/kWh)				
Case I	623	6.48	2.88	0.1083	632.468	22,311.93	8612.76	61.40%
Case II						22,250.02	7898.54	64.50%
Case III						22,452.26	8761.12	60.98%
Modified IEEE 69 Unbalanced case								
Case I	623	6.48	2.88	0.1083	632.468	22,409.90	9513.67	57.55%
Case II						22,341.29	8849.41	60.39%
Case III						22,582.49	8402.40	62.79%

Table 15. Comparison of distribution system efficiency for different cases.

Comparative Analysis		Total Power Demand (MVA)	Total Power Loss without DG and EV (MVA)	Total Power Loss with DG and EV (MVA)	System Efficiency without DG and EV	System Efficiency with DG and EV
IEEE 69 Balance	Case I	4660.214	247.1118	12.81775	95.27%	99.71%
	Case II	4660.214	234.3301	11.83228	95.51%	99.73%
	Case III	4660.214	346.0794	12.12804	92.75%	99.70%
Modified IEEE 69 Unbalance	Case I	4660.214	267.3221	25.55506	94.34%	99.46%
	Case II	4660.214	253.1297	23.48099	94.62%	99.51%
	Case III	4660.214	378.5953	28.55009	92.79%	99.42%

6. Conclusions

This study analyzed and evaluated three cases of unbalanced and balanced load distributions on an IEEE 69 bus, taking into account global average temperature changes during the day and night. Temperature variations affect system performance parameters, showing the complexity of the present configuration. This study proposes EV charging stations with optimal DG location with 3.64% EV load penetration. Here, DG mitigates the impact of the load on EV charging stations. In all cases, greenhouse gas emissions are lowered by 60.98–64.5% in the balanced scenario and 57.55–62.79% in the unbalanced scenario. The annual cost of energy loss was minimized by almost 96% in balance and almost 92% in unbalanced network in all the cases after the DG and EV integration in the test bus network. This study's multi-objective function is employed to figure out the optimal bus location along with the size of distributed DG and EV. The incorporation of DG and EV into the present network lowered both reactive and active power loss. This variation in global temperature comparison research demonstrates the technological, economic, and environmental impacts of balanced versus unbalanced networks. The main characteristic of unbalanced systems is voltage stability, which is reduced, and the system becomes more complex when compared to balance. The optimal location of DG and EV also varies with unbalanced load distribution. The CEL and GHG savings are similarly diminished when operating the same load in an imbalanced situation. Active and reactive power losses are increased, and the size of the DG and cost are increased. However, it can be concluded that if any network needs reconstruction with DG and EV, the unbalancing effect of the load must always be considered. Performance, like efficiency, stability, and losses are also affected by temperature variation under balanced and unbalanced conditions.

Author Contributions: Conceptualization, investigation, methodology, original draft preparation and validation, A.K.; Visualization, supervision, software and formal analysis, S.K.; resources, supervision and data curation, U.K.S.; writing—review and editing, A.K.B. All authors have read and agreed to the published version of the manuscript.

Funding: This research received no external funding.

Data Availability Statement: The original contributions presented in the study are included in the article, further inquiries can be directed to the corresponding author.

Conflicts of Interest: The authors declare no conflicts of interest.

Abbreviations

DG	Distributed Generation
EV	Electric Vehicle
PSO	Particle Swarm Optimization
VDI	Voltage Deviation Index
CEL	Cost of Energy Loss
MOF	Multi-Objective Function
GHG	Greenhouse Gases
EVCS	Electric Vehicles Charging Station
DERs	Distributed Energy Resources
BES	Battery Energy Storage
DSTATCOM	Distribution Static Synchronous Compensator
PV	Photovoltaic
SoC	State of Charge
DN	Distribution Network

Appendix A. The Data of IEEE 69 Bus Three Phase Balanced and Modified Unbalanced System

IEEE 69 Balanced (Three-Phase Load Data)										Modified IEEE 69 Unbalanced (Three-Phase Load Data)							
Bus Node No.	Three-Phase Distribution	transformer Connection Type	Bus Type	Active Power (Phase A)	Reactive Power (Phase A)	Active Power (Phase B)	Reactive Power (Phase B)	Active Power (Phase C)	Reactive Power (Phase C)	Phase Distribution	Connection type	Active Power (Phase A)	Reactive Power (Phase A)	Active Power (Phase B)	Reactive Power (Phase B)	Active Power (Phase C)	Reactive Power (Phase C)
1	ABC	Y	slack	0	0	0	0	0	0	ABC	Y	0	0	0	0	0	0
2	ABC	Y	PQ	0	0	0	0	0	0	ABC	Y	0	0	0	0	0	0
3	ABC	Y	PQ	0	0	0	0	0	0	ABC	Y	0	0	0	0	0	0
4	ABC	Y	PQ	0	0	0	0	0	0	ABC	Y	0	0	0	0	0	0
5	ABC	Y	PQ	0	0	0	0	0	0	ABC	Y	0	0	0	0	0	0
6	ABC	Y	PQ	0.867	0.733	0.867	0.733	0.867	0.733	AB	Y	1.3	1.1	1.3	1.1	0	0
7	ABC	Y	PQ	13.467	10.000	13.467	10.000	13.467	10.000	A	D	40.4	30	0	0	0	0
8	ABC	Y	PQ	25.000	18.000	25.000	18.000	25.000	18.000	BC	Y	0	0	37.5	27	37.5	27
9	ABC	Y	PQ	10.000	7.333	10.000	7.333	10.000	7.333	B	Y	0	0	30	22	0	0
10	ABC	Y	PQ	9.333	6.333	9.333	6.333	9.333	6.333	C	Y	0	0	0	0	28	19
11	ABC	Y	PQ	48.333	34.667	48.333	34.667	48.333	34.667	ABC	Y	48.33	34.67	48.33	34.67	48.33	34.67
12	ABC	Y	PQ	48.333	34.667	48.333	34.667	48.333	34.667	ABC	Y	48.33	34.67	48.33	34.67	48.33	34.67
13	ABC	Y	PQ	2.667	1.833	2.667	1.833	2.667	1.833	A	Y	8	5.5	0	0	0	0
14	ABC	Y	PQ	2.667	1.833	2.667	1.833	2.667	1.833	B	Y	0	0	8	5.5	0	0
15	ABC	Y	PQ	0.000	0.000	0.000	0.000	0.000	0.000	ABC	Y	0	0	0	0	0	0
16	ABC	Y	PQ	15.167	10.000	15.167	10.000	15.167	10.000	C	Y	0	0	0	0	45.5	30
17	ABC	Y	PQ	20.000	11.667	20.000	11.667	20.000	11.667	A	Y	60	35	0	0	0	0
18	ABC	Y	PQ	20.000	11.667	20.000	11.667	20.000	11.667	B	Y	0	0	60	35	0	0
19	ABC	Y	PQ	0.000	0.000	0.000	0.000	0.000	0.000	ABC	Y	0	0	0	0	0	0
20	ABC	Y	PQ	0.333	0.200	0.333	0.200	0.333	0.200	AC	Y	0.5	0.3	0	0	0.5	0.3
21	ABC	Y	PQ	38.000	27.000	38.000	27.000	38.000	27.000	C	Y	0	0	0	0	114	81
22	ABC	Y	PQ	1.767	1.167	1.767	1.167	1.767	1.167	A	Y	5.3	3.5	0	0	0	0
23	ABC	Y	PQ	0.000	0.000	0.000	0.000	0.000	0.000	ABC	Y	0	0	0	0	0	0
24	ABC	Y	PQ	9.333	6.667	9.333	6.667	9.333	6.667	B	Y	0	0	28	20	0	0
25	ABC	Y	PQ	0.000	0.000	0.000	0.000	0.000	0.000	ABC	D	0	0	0	0	0	0
26	ABC	Y	PQ	4.667	3.333	4.667	3.333	4.667	3.333	C	Y	0	0	0	0	14	10
27	ABC	Y	PQ	4.667	3.333	4.667	3.333	4.667	3.333	A	Y	14	10	0	0	0	0

IEEE 69 Balanced (Three-Phase Load Data)											Modified IEEE 69 Unbalanced (Three-Phase Load Data)						
Bus Node No.	**Three-Phase Distri-bution**	**transformer Connec-tion Type**	**Bus Type**	**Active Power (Phase A)**	**Reactive Power (Phase A)**	**Active Power (Phase B)**	**Reactive Power (Phase B)**	**Active Power (Phase C)**	**Reactive Power (Phase C)**	**Phase Distri-bution**	**Connection type**	**Active Power (Phase A)**	**Reactive Power (Phase A)**	**Active Power (Phase B)**	**Reactive Power (Phase B)**	**Active Power (Phase C)**	**Reactive Power (Phase C)**
28	ABC	Y	PQ	8.667	6.200	8.667	6.200	8.667	6.200	B	Y	0	0	26	18.6	0	0
29	ABC	Y	PQ	8.667	6.200	8.667	6.200	8.667	6.200	C	Y	0	0	0	0	26	18.6
30	ABC	Y	PQ	0.000	0.000	0.000	0.000	0.000	0.000	ABC	Y	0	0	0	0	0	0
31	ABC	Y	PQ	0.000	0.000	0.000	0.000	0.000	0.000	ABC	Y	0	0	0	0	0	0
32	ABC	Y	PQ	0.000	0.000	0.000	0.000	0.000	0.000	ABC	Y	0	0	0	0	0	0
33	ABC	Y	PQ	4.667	3.333	4.667	3.333	4.667	3.333	A	Y	14	10	0	0	0	0
34	ABC	Y	PQ	6.500	4.667	6.500	4.667	6.500	4.667	B	Y	0	0	19.5	14	0	0
35	ABC	Y	PQ	2.000	1.333	2.000	1.333	2.000	1.333	ABC	Y	2	1.33	2	1.33	2	1.33
36	ABC	Y	PQ	0.000	0.000	0.000	0.000	0.000	0.000	ABC	Y	0	0	0	0	0	0
37	ABC	Y	PQ	26.333	18.800	26.333	18.800	26.333	18.800	ABC	Y	26.34	18.8	26.34	18.8	26.34	18.8
38	ABC	Y	PQ	128.233	91.500	128.233	91.500	128.233	91.500	C	Y	0	0	0	0	384.7	274.5
39	ABC	Y	PQ	128.233	91.500	128.233	91.500	128.233	91.500	A	Y	384.7	274.5	0	0	0	0
40	ABC	Y	PQ	13.500	9.433	13.500	9.433	13.500	9.433	B	D	0	0	40.5	28.3	0	0
41	ABC	Y	PQ	1.200	0.900	1.200	0.900	1.200	0.900	AB	Y	1.8	1.35	1.8	1.35	0	0
42	ABC	Y	PQ	1.450	1.167	1.450	1.167	1.450	1.167	C	Y	0	0	0	0	4.35	3.5
43	ABC	Y	PQ	8.800	6.333	8.800	6.333	8.800	6.333	BC	Y	0	0	13.2	9.5	13.2	9.5
44	ABC	Y	PQ	8.000	5.733	8.000	5.733	8.000	5.733	ABC	Y	8	5.73	8	5.73	8	5.73
45	ABC	Y	PQ	0.000	0.000	0.000	0.000	0.000	0.000	ABC	Y	0	0	0	0	0	0
46	ABC	Y	PQ	0.000	0.000	0.000	0.000	0.000	0.000	ABC	Y	0	0	0	0	0	0
47	ABC	Y	PQ	0.000	0.000	0.000	0.000	0.000	0.000	ABC	Y	0	0	0	0	0	0
48	ABC	Y	PQ	33.333	24.000	33.333	24.000	33.333	24.000	A	Y	100	72	0	0	0	0
49	ABC	Y	PQ	0.000	0.000	0.000	0.000	0.000	0.000	ABC	Y	0	0	0	0	0	0
50	ABC	Y	PQ	414.667	296.000	414.667	296.000	414.667	296.000	ABC	Y	414.66	296	414.66	296	414.66	296
51	ABC	Y	PQ	10.667	7.667	10.667	7.667	10.667	7.667	AB	Y	16	11.5	16	11.5	0	0
52	ABC	Y	PQ	0.000	0.000	0.000	0.000	0.000	0.000	ABC	Y	0	0	0	0	0	0
53	ABC	Y	PQ	75.667	54.000	75.667	54.000	75.667	54.000	A	Y	227	162	0	0	0	0
54	ABC	Y	PQ	19.667	14.000	19.667	14.000	19.667	14.000	BC	Y	0	0	29.5	21	29.5	21
55	ABC	Y	PQ	6.000	4.333	6.000	4.333	6.000	4.333	B	Y	0	0	18	13	0	0
56	ABC	Y	PQ	6.000	4.333	6.000	4.333	6.000	4.333	C	Y	0	0	0	0	18	13

IEEE 69 Balanced (Three-Phase Load Data)											Modified IEEE 69 Unbalanced (Three-Phase Load Data)						
Bus Node No.	**Three-Phase Distribution**	**transformer Connection Type**	**Bus Type**	**Active Power (Phase A)**	**Reactive Power (Phase A)**	**Active Power (Phase B)**	**Reactive Power (Phase B)**	**Active Power (Phase C)**	**Reactive Power (Phase C)**	**Phase Distribution**	**Connection type**	**Active Power (Phase A)**	**Reactive Power (Phase A)**	**Active Power (Phase B)**	**Reactive Power (Phase B)**	**Active Power (Phase C)**	**Reactive Power (Phase C)**
57	ABC	Y	PQ	9.333	6.667	9.333	6.667	9.333	6.667	ABC	Y	9.33	6.66	9.33	6.66	9.33	6.66
58	ABC	Y	PQ	9.333	6.667	9.333	6.667	9.333	6.667	ABC	D	9.34	6.67	9.34	6.67	9.34	6.67
59	ABC	Y	PQ	8.667	6.183	8.667	6.183	8.667	6.183	A	Y	26	18.55	0	0	0	0
60	ABC	Y	PQ	8.667	6.183	8.667	6.183	8.667	6.183	B	Y	0	0	26	18.55	0	0
61	ABC	Y	PQ	0.000	0.000	0.000	0.000	0.000	0.000	ABC	Y	0	0	0	0	0	0
62	ABC	Y	PQ	8.000	5.667	8.000	5.667	8.000	5.667	C	Y	0	0	0	0	24	17
63	ABC	Y	PQ	8.000	5.667	8.000	5.667	8.000	5.667	A	Y	24	17	0	0	0	0
64	ABC	Y	PQ	0.400	0.333	0.400	0.333	0.400	0.333	B	Y	0	0	1.2	1	0	0
65	ABC	Y	PQ	0.000	0.000	0.000	0.000	0.000	0.000	ABC	Y	0	0	0	0	0	0
66	ABC	Y	PQ	2.000	1.433	2.000	1.433	2.000	1.433	AC	Y	3	2.15	0	0	3	2.15
67	ABC	Y	PQ	0.000	0.000	0.000	0.000	0.000	0.000	ABC	Y	0	0	0	0	0	0
68	ABC	Y	PQ	13.073	8.767	13.073	8.767	13.073	8.767	C	Y	0	0	0	0	39.22	26.3
69	ABC	Y	PQ	13.073	8.767	13.073	8.767	13.073	8.767	A	Y	39.22	26.3	0	0	0	0

References

1. Rajendran, G.; Vaithilingam, C.A.; Misron, N.; Naidu, K.; Ahmed, R. A comprehensive review on system architecture and international standards for electric vehicle charging stations. *J. Energy Storage* **2021**, *42*, 103099. [CrossRef]
2. Kathiravan, K.; Rajnarayanan, P.N. Application of AOA algorithm for optimal placement of electric vehicle charging station to minimize line losses. *Electr. Power Syst. Res.* **2023**, *214*, 108868. [CrossRef]
3. Rajani, B.; Kommula, B.N. An optimal energy management among the electric vehicle charging stations and electricity distribution system using GPC-RERNN approach. *Energy* **2022**, *245*, 123180. [CrossRef]
4. Ahmad, F.; Iqbal, A.; Ashraf, I.; Marzband, M. Optimal location of electric vehicle charging station and its impact on distribution network: A review. *Energy Rep.* **2022**, *8*, 2314–2333. [CrossRef]
5. Ahmad, F.; Ashraf, I.; Iqbal, A.; Marzband, M.; Khan, I. A novel AI approach for optimal deployment of EV fast charging station and reliability analysis with solar based DGs in distribution network. *Energy Rep.* **2022**, *8*, 11646–11660. [CrossRef]
6. Toghranegar, S.; Rabiee, A.; Soroudi, A. Enhancing the unbalanced distribution network's hosting capacity for DERs via optimal load re-phasing. *Sustain. Cities Soc.* **2022**, *87*, 104243. [CrossRef]
7. Abujubbeh, M.; Natarajan, B. A New Probabilistic Framework for EV Charging Station Planning in Distribution Systems Considering Spatio-temporal Uncertainties. In Proceedings of the 2023 IEEE Kansas Power and Energy Conference (KPEC), Manhattan, KS, USA, 27–28 April 2023; IEEE: Piscataway, NJ, USA, 2023; pp. 1–6.
8. Harish, B.N.; Surendra, U. A review on power quality issues in electric vehicle interfaced distribution system and mitigation techniques. *Indones. J. Electr. Eng. Comput. Sci.* **2022**, *25*, 656–665. [CrossRef]
9. Ahmad, F.; Khalid, M.; Panigrahi, B.K. An enhanced approach to optimally place the solar powered electric vehicle charging station in distribution network. *J. Energy Storage* **2021**, *42*, 103090. [CrossRef]
10. Eid, A.; Mohammed, O.; El-Kishky, H. Efficient operation of battery energy storage systems, electric-vehicle charging stations and renewable energy sources linked to distribution systems. *J. Energy Storage* **2022**, *55*, 105644. [CrossRef]
11. Islam, M.S.; Mithulananthan, N.; Hung, D.Q. Coordinated EV charging for correlated EV and grid loads and PV output using a novel, correlated, probabilistic model. *Int. J. Electr. Power Energy Syst.* **2018**, *104*, 335–348. [CrossRef]
12. Jha, B.K.; Singh, A.; Kumar, A.; Misra, R.K.; Singh, D. Phase unbalance and PAR constrained optimal active and reactive power scheduling of Virtual Power Plants (VPPs). *Int. J. Electr. Power Energy Syst.* **2020**, *125*, 106443. [CrossRef]
13. Esmaili, M.; Goldoust, A. Multi-objective optimal charging of plug-in electric vehicles in unbalanced distribution networks. *Int. J. Electr. Power Energy Syst.* **2015**, *73*, 644–652. [CrossRef]
14. AbuElrub, A.; Hamed, F.; Saadeh, O. Microgrid integrated electric vehicle charging algorithm with photovoltaic generation. *J. Energy Storage* **2020**, *32*, 101858. [CrossRef]
15. Kumar, A.; Kumar, S.; Sinha, U.K.; Bohre, A.K. Renewable DG Integration in the Unbalanced Distribution System with Impact of EV Penetration for Sustainable Operation. In Proceedings of the 2023 IEEE 3rd International Conference on Smart Technologies for Power, Energy and Control (STPEC), Bhubaneswar, India, 10–13 December 2023; IEEE: Piscataway, NJ, USA, 2023; pp. 1–6.
16. Balu, K.; Mukherjee, V. Optimal allocation of electric vehicle charging stations and renewable distributed generation with battery energy storage in radial distribution system considering time sequence characteristics of generation and load demand. *J. Energy Storage* **2023**, *59*, 106533. [CrossRef]
17. Ren, X.; Zhang, H.; Hu, R.; Qiu, Y. Location of electric vehicle charging stations: A perspective using the grey decision-making model. *Energy* **2019**, *173*, 548–553. [CrossRef]
18. Shivashankar, G.S. Overview of different overhead transmission line conductors. *Mater. Today Proc.* **2017**, *4*, 11318–11324.
19. Karmakar, S.; Bera, T.K.; Bohre, A.K. Novel PI controller and ANN controllers-Based passive cell balancing for battery management system. *IEEE Trans. Ind. Appl.* **2023**, *59*, 7623–7634. [CrossRef]
20. Burle, T.; Chintapalli, V.B.R. Modified load flow algorithm suitable for modern power systems under variable weather conditions. *Electr. Power Syst. Res.* **2022**, *211*, 108221. [CrossRef]
21. Xu, Q.; Zhang, H.; Cao, Y.; Qin, H.; Gao, Z. Power System State Estimation Approach Considering Transmission Line Temperature. *Appl. Sci.* **2022**, *12*, 10171. [CrossRef]
22. Haldar, S.; Choudhury, M.; Choudhury, S.; Samanta, P. Trend analysis of long-term meteorological data of a growing metropolitan city in the era of global climate change. *Total Environ. Res. Themes* **2023**, *7*, 100056. [CrossRef]
23. Albrechtowicz, P. The overhead transmission line temperature impact on the phase-shifting transformer settings. *Electr. Power Syst. Res.* **2023**, *220*, 109266. [CrossRef]
24. Cecchi, V.; Knudson, M.; Miu, K. System impacts of temperature-dependent transmission line models. *IEEE Trans. Power Deliv.* **2013**, *28*, 2300–2308. [CrossRef]
25. Dong, X.; Wang, C.; Liang, J.; Han, X.; Zhang, F.; Sun, H.; Wang, M.; Ren, J. Calculation of power transfer limit considering electro-thermal coupling of overhead transmission line. *IEEE Trans. Power Syst.* **2014**, *29*, 1503–1511. [CrossRef]
26. Burle, T.; Chintapalli, V.B.R. Effect of ambient temperature variations on estimation of proximity of the voltage collapse point. *IET Gener. Transm. Distrib.* **2020**, *14*, 6382–6396. [CrossRef]
27. Mishra, A.; Rajan, J.S. Development of a Self-Powered Temperature Monitoring Wireless Node for Transmission Lines for Smart Grid Application. *Power Res. A J. CPRI* **2019**, *14*, 93–103. [CrossRef]
28. Rahman, M.; Atchison, F.; Cecchi, V. Temperature-dependent system level analysis of electric power transmission systems: A review. *Electr. Power Syst. Res.* **2021**, *193*, 107033. [CrossRef]

29. Rakpenthai, C.; Uatrongjit, S. Power system state and transmission line conductor temperature estimation. *IEEE Trans. Power Syst.* **2016**, *32*, 1818–1827. [CrossRef]
30. Koufakis, E.I.; Tsarabaris, P.T.; Katsanis, J.S.; Karagiannopoulos, C.G.; Bourkas, P.D. A wildfire model for the estimation of the temperature rise of an overhead line conductor. *IEEE Trans. Power Deliv.* **2010**, *25*, 1077–1082. [CrossRef]
31. Valentina, C.; St, L.A.; Karen, M. Incorporating temperature variations into transmission-line models. *IEEE Trans. Power Deliv.* **2011**, *26*, 2189–2196.
32. Bockarjova, M.; Andersson, G. Transmission line conductor temperature impact on state estimation accuracy. In Proceedings of the 2007 IEEE Lausanne Power Tech, Lausanne, Switzerland, 1–5 July 2007; IEEE: Piscataway, NJ, USA, 2007; pp. 701–706.
33. Du, Y.; Liao, Y. On-line estimation of transmission line parameters, temperature and sag using PMU measurements. *Electr. Power Syst. Res.* **2012**, *93*, 39–45. [CrossRef]
34. Leger, A.S.; Nwankpa, C. OTA-based transmission line model with variable parameters for analog power flow computation. *Int. J. Circuit Theory Appl.* **2008**, *38*, 199–220. [CrossRef]
35. Sagiyeva, I.Y.; Nosov, A.V.; Surovtsev, R.S. The influence of temperature on microstrip transmission line characteristics. In Proceedings of the 2020 21st International Conference of Young Specialists on Micro/Nanotechnologies and Electron Devices (EDM), Chemal, Russia, 29 June–3 July 2020; IEEE: Piscataway, NJ, USA, 2020; pp. 191–194.
36. Du, Y.; Liao, Y. Online estimation of power transmission line parameters, temperature and sag. In Proceedings of the 2011 North American Power Symposium, Boston, MA, USA, 4–6 August 2011; IEEE: Piscataway, NJ, USA, 2011; pp. 1–6.
37. Moghassemi, A.; Padmanaban, S.; Ramachandaramurthy, V.K.; Mitolo, M.; Benbouzid, M. A novel solar photovoltaic fed TransZSI-DVR for power quality improvement of grid-connected PV systems. *IEEE Access* **2020**, *9*, 7263–7279. [CrossRef]
38. Satyanarayana PV, V.; Radhika, A.; Reddy, C.R.; Pangedaiah, B.; Martirano, L.; Massaccesi, A.; Jasiński, M. Combined DC-link fed parallel-VSI-based DSTATCOM for power quality improvement of a solar DG integrated system. *Electronics* **2023**, *12*, 505. [CrossRef]
39. Oda, E.S.; Abd El Hamed, A.M.; Ali, A.; Elbaset, A.A.; Abd El Sattar, M.; Ebeed, M. Stochastic optimal planning of distribution system considering integrated photovoltaic-based DG and DSTATCOM under uncertainties of loads and solar irradiance. *IEEE Access* **2021**, *9*, 26541–26555. [CrossRef]
40. Souza, P.A.; Santos GB, D.; Mariano, V.; Barbosa, D. Analysis of active and reactive power injection in distributed systems with photovoltaic generation. In Proceedings of the 2018 Simposio Brasileiro de Sistemas Eletricos (SBSE), Niteroi, Brazil, 12–16 May 2018; IEEE: Piscataway, NJ, USA, 2018; pp. 1–6.
41. Albuquerque, F.L.; Moraes, A.J.; Guimarães, G.C.; Sanhueza, S.M.; Vaz, A.R. Photovoltaic solar system connected to the electric power grid operating as active power generator and reactive power compensator. *Sol. Energy* **2010**, *84*, 1310–1317. [CrossRef]
42. Zubo, R.H.; Mokryani, G.; Abd-Alhameed, R. Optimal operation of distribution networks with high penetration of wind and solar power within a joint active and reactive distribution market environment. *Appl. Energy* **2018**, *220*, 713–722. [CrossRef]
43. Paghdar, S.; Sipai, U.; Ambasana, K.; Chauhan, P.J. Active and reactive power control of grid connected distributed generation system. In Proceedings of the 2017 Second International Conference on Electrical, Computer and Communication Technologies (ICECCT), Coimbatore, India, 22–24 February 2017; IEEE: Piscataway, NJ, USA, 2017; pp. 1–7.
44. Vincze, M.; Borcia, I.D.; Harlander, U. Temperature fluctuations in a changing climate: An ensemble-based experimental approach. *Sci. Rep.* **2017**, *7*, 254. [CrossRef]
45. Gyüre, B.; Bartos, I.; Jánosi, I.M. Nonlinear statistics of daily temperature fluctuations reproduced in a laboratory experiment. *Phys. Rev. E* **2007**, *76*, 037301. [CrossRef]
46. Kim, I.Y.; de Weck, O.L. Adaptive weighted sum method for multiobjective optimization: A new method for Pareto front generation. *Struct. Multidiscip. Optim.* **2005**, *31*, 105–116. [CrossRef]
47. Jin, J.; Rothrock, L.; McDermott, P.L.; Barnes, M. Using the Analytic Hierarchy Process to Examine Judgment Consistency in a Complex Multiattribute Task. *IEEE Trans. Syst. Man Cybern. Part A Syst. Hum.* **2010**, *40*, 1105–1115. [CrossRef]
48. Khan, S.; Ahmad, A.; Ahmad, F.; Shemami, M.S.; Alam, M.S.; Khateeb, S. A comprehensive review on solar powered electric vehicle charging system. *Smart Sci.* **2017**, *6*, 54–79. [CrossRef]
49. Prasad, C.H.; Subbaramaiah, K.; Sujatha, P. Cost–benefit analysis for optimal DG placement in distribution systems by using elephant herding optimization algorithm. *Renew. Wind. Water Sol.* **2019**, *6*, 1–12. [CrossRef]
50. Rani, K.; Acharjee, P.; Bohre, A. Determining Optimal Size and Placement of Renewable DG Considering Variation of Load. *Int. J. Recent Technol. Eng.* **2019**, *8*, 310–315. [CrossRef]
51. Elsheikh, A.H.; Abd Elaziz, M. Review on applications of particle swarm optimization in solar energy systems. *Int. J. Environ. Sci. Technol.* **2018**, *16*, 1159–1170. [CrossRef]
52. Bohre, A.K.; Acharjee, P.; Sawle, Y. Analysis of grid connected hybrid micro-grid with different utility tariffs. In Proceedings of the 2021 1st International Conference on Power Electronics and Energy (ICPEE), Bhubaneswar, India, 2–3 January 2021; IEEE: Piscataway, NJ, USA, 2021; pp. 1–6.
53. Dincer, F. The analysis on photovoltaic electricity generation status, potential and policies of the leading countries in solar energy. *Renew. Sustain. Energy Rev.* **2011**, *15*, 713–720. [CrossRef]
54. Thangavel, S.; Mohanraj, D.; Girijaprasanna, T.; Raju, S.; Dhanamjayulu, C.; Muyeen, S.M. A comprehensive review on electric vehicle: Battery management system, charging station, traction motors. *IEEE Access* **2023**, *11*, 20994–21019. [CrossRef]

55. Chen, T.-H.; Chen, M.-S.; Inoue, T.; Kotas, P.; Chebli, E.A. Three-phase co-generator and transformer models for distribution system analysis. *IEEE Trans. Power Deliv.* **1991**, *6*, 1671–1681. [CrossRef]
56. Kumar, A.; Kumar, S.; Sinha, U.K.; Saw, B.K.; Bohre, A.K. Integration of Green Renewable DG based EV Charging Stations Planning in Unbalanced Distribution Network. In Proceedings of the 2023 IEEE International Conference on Power Electronics, Smart Grid, and Renewable Energy (PESGRE), Trivandrum, India, 17–20 December 2023; IEEE: Piscataway, NJ, USA, 2023; pp. 1–6.